



Economic lifetime-aware wind farm control

Abhinav Anand, Robert Braunbehrens, Adrien Guilloré, and Carlo L. Bottasso

Technical University of Munich, Wind Energy Institute, Boltzmannstraße 15, 85748 Garching b. München, Germany

Abstract.

We present the economic lifetime-aware formulation of wind farm control (WFC), a novel approach that incorporates the current state of damage of turbines – either provided by a digital twin or estimated from operational data – to compute control policies that optimize the long-term life management of a wind farm. The optimization is guided by an economic value function that balances power capture (taking into account variable spot market prices) with operation and maintenance (O&M) costs, including potential revenue losses due to turbine downtime. The optimization process is subject to constraints ensuring that the target lifetime of selected turbine components is met, considering varying inflow conditions. This results in optimal control setpoints for each turbine as functions of ambient conditions.

After introducing the economic lifetime-aware WFC approach, the paper analyzes two case studies. The first is a synthetic scenario with a simplified set of environmental conditions, designed to demonstrate the behavior of the new control strategy and its impact on fatigue loads. The second case features the more realistic setup of a small wind farm, with wind climate data derived from a real meteorological mast. The benefits of the proposed methodology are highlighted by comparing it to a range of reference control strategies, which either ignore component damage or address fatigue loads in alternative simplified ways. When compared to greedy and power-maximizing WFC strategies, results show that only the lifetime-aware formulation ensures the achievement of the desired lifetime targets. Additionally, it also results in the best economic performance.

1 Introduction

Most current wind farm control (WFC) strategies focus on increasing power generation (Meyers et al., 2022). However, this is only one of several goals of the more general concept of optimal operation. In fact, a wind energy project sits in a complex dynamic environment and has various stakeholders. External factors, such as electricity market price or grid loads and transmission constraints, continuously evolve over time. This variation has a dynamic impact on the value of the wind farm power output being fed into the grid. For example, in some cases, it pays off to extract maximum yield from the farm. In contrast, in other cases, generating less will be more convenient because of low electricity prices that cannot offset the incurred costs. Within the farm itself, every control action will affect the internal response of the system, e.g. by changing the loading on the turbines and their components. In turn, this affects the turbine “health”, directly influencing the overall asset lifetime and the repair and maintenance activities needed during its operation. Considering these factors and couplings, it seems hardly optimal to feed in maximum power to the grid at all times. To successfully optimize a wind energy project, the scope needs to be



expanded towards a more holistic view. New formulations of WFC need to be able to incorporate, on the one hand, all relevant external requirements and conditions and, on the other, the internal response of the system.

During operation, wind turbines incur fatigue damage, i.e. structural degradation in their components such as tower, blades, drive-train, and others (Anand et al., 2022). After accruing a limiting damage value, the asset is considered to have reached its end of life (EOL). Flow control strategies modify the inflow conditions within the farm, either by derating the turbines, by misaligning them with respect to the wind, or by applying excitations meant to accelerate wake recovery (Meyers et al., 2022). Therefore, a farm control policy affects the rate at which damage accrues in the turbine components. This, in turn, has a direct effect on the asset lifetime, potentially limiting or extending the project duration and affecting the economic profitability of the wind farm. Thus, wind turbine fatigue damage plays a crucial role in determining the performance of a farm control policy. Some initial efforts at including fatigue in wind farm control have already been documented (Harrison et al., 2020b; Eguinoa et al., 2021; Dimitrov and Natarajan, 2021). Such control strategies typically try to restrict damage equivalent loads (DELs) by either setting a limiting value or by considering them directly in an additional objective. However, such choices can hardly lead to a clear understanding of the effects of the resulting control policies on lifetime. In fact, damage accrues over time, and therefore, the control actions taken today – through the loading of the turbines – directly affect the room left for control actions that can be taken in the future. Thus, optimizing the operation of a wind farm over its lifetime cannot only rest on decisions based on present conditions or over short time horizons. Instead, one needs to consider the couplings between present and future actions.

This work presents a new form of WFC, termed economic lifetime-aware WFC. The formulation incorporates the current state of damage of the turbines – either provided by a digital twin or estimated from operational data – to compute control policies that optimize the long-term life management of the wind farm. The optimization is guided by an economic value function that balances power capture (taking into account variable spot market prices) with operation and maintenance (O&M) costs, including potential revenue losses due to turbine downtime. The optimization process is subject to constraints ensuring that the target lifetime of selected turbine components is met, considering varying inflow conditions. The optimization variables are the control setpoints of each turbine. The selection of the control variables depends on the specific WFC implementation chosen: induction-based control to reduce wake intensity, yaw-offset-based control for wake steering, or a combination of both. Although mixing is yet another flow control method, it was not considered in the scope of the present work. The proposed methodology is versatile and can be applied to any WFC implementation, allowing the end user to choose based on their preferences and the trade-offs offered by different control strategies. The outputs of the WFC optimization problem are the optimal setpoints for each turbine in the farm as functions of ambient condition. Although sophisticated dynamic (model predictive) approaches are possible and indeed promising (van den Broek et al., 2024), the present relatively simpler implementation based on offline-computed look-up tables is very close to the power-boosting WFC technology already successfully implemented by industry.

Compared to existing approaches, the novelty of the proposed WFC methodology lies in incorporating the desired wind farm lifetime as an optimization constraint and using an economic merit function as the optimization objective. While this paper highlights the combined use of these two innovations, they can also be applied separately. If component damage is not



a major concern (for instance, at a site with a mild environment relative to the turbine design limits), the lifetime constraint can be omitted, while still using the economic value function to drive the optimization. This reduces the computational cost, while still offering a clearer optimization goal over existing formulations that blend power production and loads with arbitrary weighting factors (Harrison et al., 2020b). Alternatively, a different (future better) economic merit function can be used, than
65 the simple one adopted here, while still maintaining the fatigue constraint to ensure that the wind farm meets the desired target lifetime.

This new economic lifetime-aware control framework allows wind farm developers in a pre-deployment phase to make informed decisions on the economic viability of various alternative operational scenarios. For instance, a developer could
70 compare a shorter lifetime duration of the plant due to higher power capture (but also higher loading and hence higher O&M costs) followed by decommissioning vs. an extension of the plant lifetime beyond its initial intended duration thanks to a less aggressive capture and less loading. Moreover, once an optimal life management strategy has been selected, the wind farm operator can deploy the lifetime-aware controller to operate the turbines in a profit-optimal way, while ensuring that the specified lifetime goals for the turbine components are met.

75 An experimental validation of the proposed WFC methodology was recently conducted by wind tunnel tests (Braunbehrens et al., 2024). The experiment involved three model turbines in a boundary layer wind tunnel, where a turntable was used to simulate dynamic variations in wind direction. The control strategy, based on wake steering, was synthesized using power and damage estimators. The proposed strategy was compared to conventional greedy operation and the classical maximum power strategy. Results showed how the new control approach not only improved the economic performance of the wind farm, but also
80 ensured operation over the desired lifetime. In this paper, we develop a more detailed description of economic lifetime-aware WFC than the one of Braunbehrens et al. (2024), and we demonstrate the new method in a simulation environment.

The rest of this paper is organized as follows. The proposed economic lifetime-aware WFC is presented in Sect. 2. This is followed by a detailed description of the optimization framework in Sect. 3, together with its supporting tools. Next, the proposed strategy and a few reference WFC formulations are applied to two case studies in Sect. 4, considering various performance
85 indicators, including power, loads, and lifetime duration. The section includes a discussion on the results, comparisons with the reference alternative formulations, and an evaluation of the computational burden. Finally, conclusions and key findings are discussed in Sect. 5.

2 Optimization problem

A standard power-capture optimal wind farm controller is typically designed by independently optimizing each ambient condition (Campagnolo et al., 2020; Göçmen et al., 2022; Howland et al., 2019). The assumption behind this approach is that
90 optimizing each condition will ultimately maximize the overall performance over time. In the case of power, this is straightforward as the produced energy over time can easily be summed up. However, designing a lifetime fatigue-optimal wind farm controller requires a different approach. Fatigue damage in a turbine component accumulates in a complex way over its lifespan, influenced by all ambient conditions encountered. Consequently, the damage accumulated under various wind conditions



95 directly affects the remaining operational life of the turbine. As a result, a lifetime fatigue-aware wind farm controller must be optimized holistically, taking into account the entire spectrum of ambient conditions throughout the lifetime of the turbines. Additionally, fatigue damage can significantly impact both the failure rate and the frequency of maintenance activities (Wilkinson et al., 2010; Scheu et al., 2017). This not only increases maintenance costs but also leads to economic losses because of the reduced power production during repair and maintenance periods.

100 The proposed WFC formulation is designed to optimize wind farm operations over its entire lifetime. The consideration of lifetime effects is integrated into the optimization problem in two ways. First, the proposed optimization ensures that the turbines operate for a specified duration without exceeding a predefined fatigue damage threshold. This threshold may represent the design lifetime of the turbine or a desired fraction of the remaining useful life, depending on the goals of the wind farm operator. This step is crucial, as failure to meet the threshold would result in revenue losses due to the reduced turbine lifespan.

105 The second aspect of the proposed optimization focuses on maximizing the overall economic profit by accounting for the impact of fatigue damage on operation and maintenance costs. This is achieved by finding trade-off between control actions aimed at increasing the economic value of power yield and those designed to mitigate the economic cost of fatigue damage. The resulting optimization provides an optimal schedule of setpoints for each turbine, tailored to the site ambient wind conditions.

This control formulation is implemented in an open-loop fashion, similarly to widely used wake-control-based power-capture optimization strategies (Campagnolo et al., 2020; Göçmen et al., 2022; Howland et al., 2019), enabling the offline application of computationally intensive one-shot optimizations through steady-state simulations.

The optimization problem can be written as

$$\max_{\mathbf{u}} \sum_T \text{Revenue}(\mathbf{W}_a, \mathbf{u}) - \text{Cost}(\mathbf{W}_a, \mathbf{u}), \quad (1a)$$

subject to

$$115 \quad D_i^c(\mathbf{W}_a, \mathbf{u}) \leq D_{\text{ref}}^c \quad \forall i \in N \text{ and } \forall c \in C, \quad (1b)$$

and

$$\mathbf{u}^{\min} \leq \mathbf{u} \leq \mathbf{u}^{\max}. \quad (1c)$$

For a given set of ambient wind conditions \mathbf{W}_a , control set-points $\mathbf{u} = [\mathbf{u}_1, \dots, \mathbf{u}_i, \dots, \mathbf{u}_N]$ for N turbines in the farm, and C components in each turbine, the optimization balances the accrued economic value through power generation $\text{Revenue}(\cdot)$ and the incurred economic cost due to maintenance activities and lost lifetime $\text{Cost}(\cdot)$, over a chosen lifetime T . The vector \mathbf{W}_a denotes the set of all wind conditions through time series of wind speeds, wind directions, and possibly other atmospheric parameters (turbulence intensity, shear), that occur over the lifetime T . In the present work, the considered ambient conditions are the hub height wind speed U , wind direction Γ , and turbulence intensity (TI) denoted as I , resulting in $\mathbf{W}_a = [U, \Gamma, I]$. Assuming the wind climate does not show any inter-annual variability, the time series can be approximated through a corresponding frequency distribution. Depending on the chosen WFC technique, the control set-point vector \mathbf{u}_i can consist of



induction factor α_i for induction control, yaw-offset γ_i for wake-steering, or a combination of the two. The optimization problem is subjected to the lifetime constraint expressed by Eq. (1b), which ensures that the resulting lifetime damage D does not exceed the damage threshold D_{ref} . This parameter is an appropriate damage limit, which includes the necessary safety factors. Clearly, there are several options for determining the limit. For instance, D_{ref} could be set to the design limit, allowing the component to be utilized up to its maximum designed capacity. Alternatively, one might leave a damage margin, ensuring that the component has a second life and extending its overall usage. Despite the various possible scenarios, the underlying concept of this approach is to maintain control over damage accumulation while pursuing a specific goal. Achieving this goal would not be possible without an explicit constraint to guide the process. In this work, for a given component c , D_{ref}^c is chosen as

$$D_{ref}^c = \max_i \sum_T D_i^c(\mathbf{W}_a) \quad \forall i \in N, \quad (2)$$

which corresponds to the maximum accumulated damage over all the turbines under the standard greedy control strategy, where no wake steering or other WFC strategies are applied. Furthermore, the optimization problem is subjected to the bound constraint Eq. (1c) on the decision variable \mathbf{u} , where \mathbf{u}^{min} and \mathbf{u}^{max} denote the lower and upper bounds, respectively.

3 Optimization framework

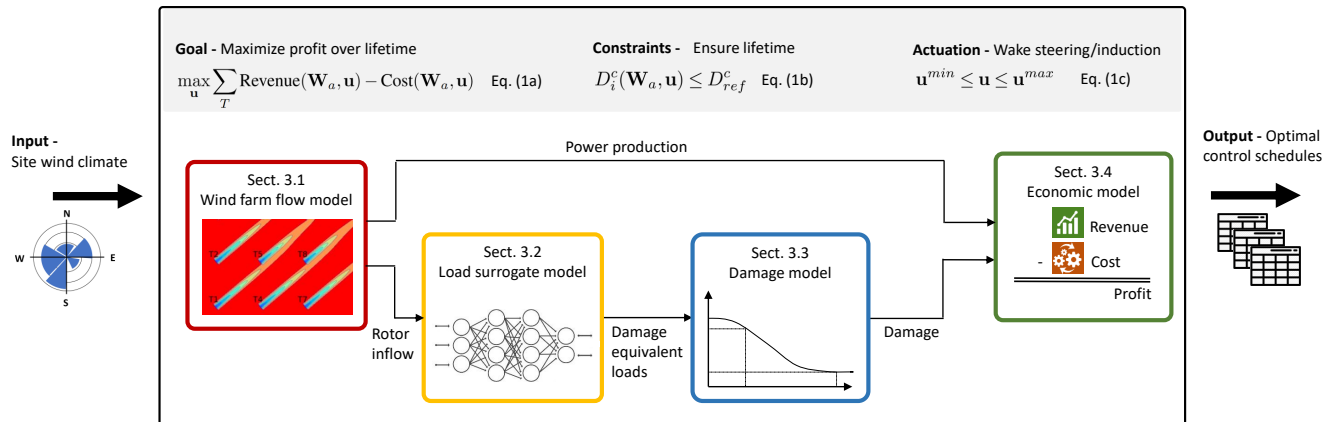


Figure 1. Optimization framework with block chart of the model toolchain.

This section describes the optimization framework designed to compute the optimal control setpoints for a wind farm using the proposed economic lifetime-aware WFC strategy. An overview of this framework, including its underlying models, is depicted in Fig. 1. The framework takes site-specific wind conditions \mathbf{W}_a as input and generates optimal control schedules $\mathbf{u}(\mathbf{W}_a)$ for all turbines in the form of look-up tables.



The equations in the grey-shaded region at the top of Fig. 1 highlight two key aspects of the proposed strategy: (i) the use of an economic merit function (Eq. 1a), and (ii) the lifetime constraint (Eq. 1b). Additionally, bounds on the control variables are enforced (Eq. 1c).
145

The underlying model set is represented by boxes with different color outlines in Fig. 1. The model toolchain consists of several components: a wind farm flow model (Sect. 3.1), a fatigue load surrogate model (Sect. 3.2), a damage estimation model (Sect. 3.3), and an economic model (Sect. 3.4).

The upper branch of the toolchain follows established research and industry practices for estimating the power production of the wind farm (Lee and Fields, 2020), which is then converted into economic revenue by the economic model. The lower branch tackles the more complex task of estimating the impact of the operational strategy on turbine components.
150

In this process, rotor inflow conditions are translated into DELs, which are then aggregated to estimate the damage to each specific component. The accumulated damage serves two purposes. First, the lifetime constraint evaluates whether the component damage is within the chosen threshold. Second, the economic model uses the accumulated damage to calculate the associated maintenance costs.
155

By combining the upper branch (revenue) and the lower branch (costs), the framework generates the economic profit metric, which is the objective of the optimization. The following subsections provide a detailed discussion of each individual model block.

3.1 Wind farm flow model

The flow model simulates wake interactions within the wind farm and maps the ambient site inflow \mathbf{W}_a to turbine-specific inflow conditions and power production. Steady-state engineering wake models offer a suitable compromise between model accuracy and computational expense, which is the reason for their widespread use within industry and research (Porté-Agel et al., 2020). Furthermore, their modular architecture and tunable parameters allow for calibrating models to better match the site conditions. The present study uses the open-source toolbox FLORIS (NREL: FLORIS, 2022). Real-world wind farm flow fields are influenced by additional factors such as terrain and farm-boundary layer interactions. Models of these effects are being developed (Stipa et al., 2024), or can be learned from operational data (Braunbehrens et al., 2023).
160
165

Figure 2a depicts the hub height flow field for an example two-turbine cluster for $\mathbf{W}_a = [8 \text{ ms}^{-1}, 275^\circ, 12\%]$. The two branches in Fig. 1 show that the flow model has two distinct outputs. First, the aggregated farm power production, a routine output of engineering wake models, is required to estimate economic revenue. Second, in the lower branch, the surrogate load model requires local wind speed and turbulence intensity conditions at each specific turbine as input. While the rotor inflow field is also available from engineering wake models, it is typically not used directly to compute loads and, therefore, needs further processing. Figure 1b illustrates the streamwise velocity field just upstream of the rotor of the second turbine, as extracted from FLORIS.
170

The Gaussian wake model used in this study captures the trend of decreasing velocity on the right side of the rotor during half-wake impingement (Bastankhah et al., 2014). In contrast, simpler submodels, such as the Jensen velocity model, would only provide a crude representation of the inflow due to their assumption of a simple top-hat profile (Katic et al., 1987). In
175

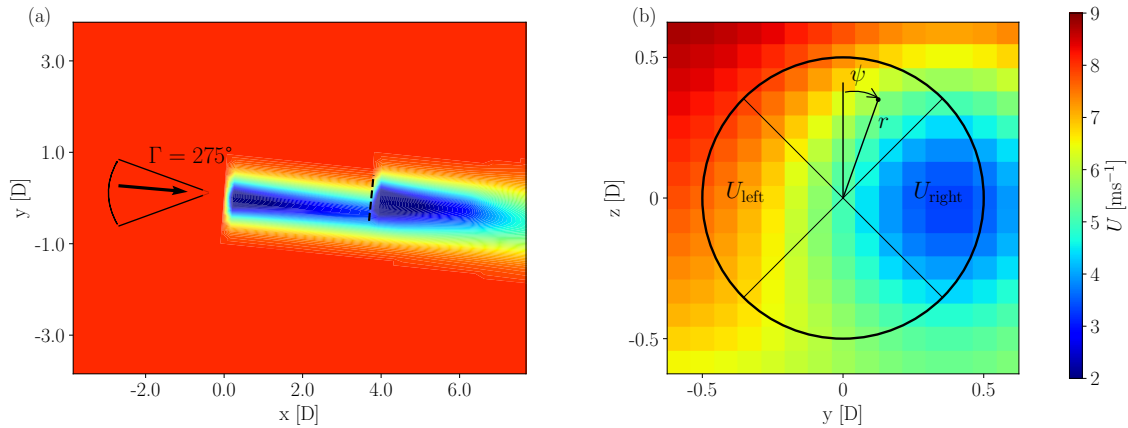


Figure 2. Streamwise velocity field for a two-turbine cluster, modelled with FLORIS. (a) horizontal plane at hub height for a wind direction $\Gamma = 275^\circ$. The indicated sector visualizes the wind direction sweep of Fig. 3. The dashed line represents the position of the vertical plane in front of the downstream turbine in panel (b). The figure includes the outline of the rotor, and its left and right quadrants used by the surrogate load model.

combination with the load model, it was observed that the baseline configuration of FLORIS does not fully capture all the necessary flow effects. The baseline wake-added turbulence by Crespo et al. (1996) are found to be inaccurate in partial wake situations, primarily due to the simplified, top-hat-like turbulence profile. To address this problem, the model was replaced
180 with the one of Ishihara and Qian (2018), which features an axisymmetric double-Gaussian TI profile. Additionally, the model equations were enhanced by making the parameters k_G , k_σ , and k_{r0} tunable, which allow for the calibration of the maximum added TI, the profile width, and the peak distance, respectively. For the velocity deficit, the Gaussian wake model by Bastankhah et al. (2014) provided a sufficiently accurate baseline for calibration. This model includes tuning parameters k_α , k_β , k_a , and k_b which, in pairs, control the far-wake onset and decay, respectively. The “wind farm as a sensor” methodology was
185 employed for the simultaneous calibration of these submodel parameters (Braunbehrens et al., 2023, 2024). The effects of these improvements are discussed next in conjunction with the load surrogate model in Sect. 3.2.3.

3.2 Load surrogate model

Following the lower branch in Fig. 1, the load model block is the second step in estimating turbine lifetime and maintenance costs. The load surrogate model predicts short-term DELs for monitored components (load channels), which are then used to
190 calculate the damage metric. Loads depend primarily on the local inflow conditions. As shown in Fig. 2b, impinging wakes significantly alter the characteristics of the incoming flow field. Additionally, loads are influenced by the control actions of the turbine. For example, performing wake steering by misaligning the upstream turbine can affect the loading of various components to a different degree (Damiani et al., 2018).



Typically, complex aero-servo-elastic simulations are required to estimate DELs at the component level. Running these
195 simulations within the optimization framework is computationally infeasible. This limitation has led to increasing interest
in load surrogates in both research and industry. Several approaches have been proposed in the literature (Dimitrov et al.,
2018; Mendez Reyes et al., 2019; Bossanyi, 2022; Shaler et al., 2022; Liew et al., 2024). However, these methods are often
site-specific, requiring retraining when the layout changes, or fail to account for the complex effects of yaw misalignment on
self-induced loads and those experienced by downstream turbines.

200 The present work adopts the load surrogate approach proposed by Guilloré et al. (2024). This surrogate is location-agnostic,
in the sense that a single model can predict loads at any turbine within an arbitrary wind farm. This surrogate is also control-
oriented, in the sense that the effect of control actions (yaw misalignment or down-regulation) on fatigue is inherently captured.

3.2.1 Model design

Given a load time series at a selected component location, DELs are estimated for a 10-minute time window using the Rainflow
205 counting algorithm and the classical formula

$$DEL = \left(\frac{\sum_i (n_i L_i^m)}{N_{eq}} \right)^{\frac{1}{m}}, \quad (3)$$

as described in Sutherland (1999) and in IEC 61400-1 (2019). Here, n_i is the number of load cycles of amplitude L_i , N_{eq} is
the equivalent number of cycles (taken conventionally to be equal to $2 \cdot 10^6$ cycles over a lifetime of 20 years), and m is the
Wöhler exponent of the S-N curve of the component material. In this work, two load channels are considered:

- 210
- Blade root: resulting from the projection of the blade root in-plane and out-of-plane bending moments along the maxi-
mum damage direction.
 - Tower base: resulting from the projection of the tower bottom fore-aft and side-side bending moments along the maxi-
mum damage direction.

The material constants were chosen as $m = 10$ for the polymer of the blades and $m = 4$ for the steel of the tower (Sutherland,
215 1999; IEC 61400-1, 2019). For the detailed methodology on projecting DELs along maximum damage direction, see Guilloré
et al. (2024).

A large number of wind farm aero-servo-elastic simulations were conducted using FAST.Farm (Jonkman and Shaler, 2021),
providing the dataset for training the machine learning surrogate model. The version of FAST.Farm used here includes an
extension proposed by Kretschmer et al. (2021), which provides a more accurate description of wake-added turbulence.

220 A total of 1,908 FAST.Farm simulations were conducted using an array of three IEA 3.4 MW reference wind turbines (Bor-
tolotti et al., 2019). The simulations consider variations of several parameters, including ambient wind speed, turbulence
intensity, wind direction, and yaw misalignment of the first two turbines. Synthetic ambient turbulent wind fields, each 10 min-
utes in length, were generated using TurbSim with the Kaimal model (Jonkman, 2016). For each simulation case, 24 turbulent
seeds were run to ensure statistical convergence. The resulting dataset was then used to train by machine learning the surrogate



225 model, which establishes a relationship between the relevant turbine inflow and operating conditions and the observed load
response.

3.2.2 Inflow characterization

The description of the turbine inflow that serves as model input has a crucial importance. Simply using the fully resolved ve-
locity field is not an ideal choice, as machine learning models tend to “learn the noise” present in the turbulence. Therefore, in
230 addition to requiring a large number of inputs, the model would perform well on the training data but poorly on test data (Guil-
loré et al., 2024). To avoid this problem, it is necessary to define suitable reduced-order quantities that minimize noise while
retaining enough information to adequately characterize the flow field.

Additionally, the inflow description must account for the fact that two models of different fidelity are used during two differ-
ent steps in the process. During dataset generation, a mid-fidelity wake meandering model (here implemented in FAST.Farm)
235 dynamically simulates the wake displacement caused by ambient eddies. The model also relies on an engineering description
of wake decay due to smaller-scale turbulence (Larsen et al., 2007). In contrast, the optimization framework uses a low-fidelity,
steady-state engineering wake model (here implemented in FLORIS) to estimate the turbine inflow, as shown for streamwise
velocity in Fig. 2b. Although both models share some similarities, the engineering model cannot produce predictions with the
same level of fidelity as the mid-fidelity model.

240 To address this problem, here we used a slightly modified version of the inflow characterization, compared to the one
presented in Guilloré et al. (2024). Instead of relying on sector-averaged inflow quantities, this work utilizes three rotor-
averaged inflow quantities (RAIQs). This approach simplifies the complex local inflow across the rotor by reducing it to
only three representative variables. Although the sector-averaged inflow quantities of Guilloré et al. (2024) offer an improved
accuracy, the present simpler approach still contains sufficient information to capture DELs. The sketch superimposed to the
245 flow field in Fig. 2b provides a visualization of the definitions of the RAIQs. The rotor-averaged wind speed (RAWS) is defined
as the mean wind speed across the rotor disk, i.e.

$$\text{RAWS} = \int_0^{2\pi} \int_0^R U(r, \psi) dr d\psi. \quad (4)$$

Here, $U(r, \psi)$ is the local wind speed at a given point, with r and ψ being the radial and azimuthal coordinates, respectively.
Similarly, the rotor-averaged turbulence intensity (RATI) is defined as the mean TI across the rotor disk and written as

$$250 \text{ RATI} = \int_0^{2\pi} \int_0^R I(r, \psi) dr d\psi, \quad (5)$$

where $I(r, \psi)$ is the local TI at a given point on the inflow plane. Finally, the rotor-averaged horizontal shear (RAHS) represents
the heterogeneity of wind speed across the rotor disk in the lateral direction. RAHS is particularly useful for characterizing
cases of full or partial wake overlap. The definition is based on Bottasso et al. (2018) and Schreiber et al. (2020), using the
left and right quadrants of the rotor disk, as visualized in Fig. 2b. The left and right quadrant-equivalent wind speeds can be



255 calculated as

$$U_{\text{right}} = \int_{\pi/4}^{3/4\pi} \int_0^R U(r, \psi) dr d\psi, \quad (6a)$$

$$U_{\text{left}} = \int_{5/4\pi}^{7/4\pi} \int_0^R U(r, \psi) dr d\psi. \quad (6b)$$

260 The horizontal shear coefficient RAHS is estimated under the assumption of a linear variation in wind speed along the lateral direction. It is further assumed that the quadrants sample the inflow at positions corresponding to $\pm 2/3$ of the rotor radius, as described by Bottasso et al. (2018) and Schreiber et al. (2020). Thus, RAHS can be calculated as

$$\text{RAHS} = \frac{3 U_{\text{right}} - U_{\text{left}}}{2 U_{\text{right}} + U_{\text{left}}}. \quad (7)$$

265 An illustrative example of the RAIQs, as estimated by the engineering wake model, is shown in the three panels of Fig. 3. The inflow situation corresponds to the downstream turbine in the example illustrated in Fig. 2, for a wind direction sweep of $250^\circ < \Gamma < 290^\circ$, where the wake of the upstream turbine makes a full pass over the downstream rotor. The ambient wind speed and TI are held constant at 8 ms^{-1} and 12%, respectively.

270 Figure 3 clearly shows that the RAWS is at its minimum for the full-wake situation ($\Gamma = 270^\circ$) and progressively recovers toward the ambient wind speed as the wind direction moves away from this value. In contrast, the RATI is largest in full-wake due to the wake-added turbulence. As the turbine experiences less wake impingement, the RATI decreases toward the ambient TI value. Finally, the RAHS shows the expected asymmetry, characteristic of left and right partial-waking. For both the full-wake ($\Gamma = 270^\circ$) and no-wake ($\Gamma < 255^\circ$ or $\Gamma > 285^\circ$) scenarios, the RAHS is close to zero, as there is no significant wind speed asymmetry across the lateral direction of the rotor disk. However, during partial-waking situations, the RAHS is positive for $255^\circ < \Gamma < 270^\circ$ and negative for $270^\circ < \Gamma < 285^\circ$. These trends in RAWS, RATI, and RAHS further contribute to the understanding of the results presented in Sect. 4.2.2.

275 3.2.3 Model performance

After establishing the inflow characterization, the surrogate load model can be synthesized from the dataset. For each simulation case and each turbine, the RAIQs were recorded from the flow field, along with the projected DELs at blade root and tower base.

280 Two artificial neural networks (ANNs) were then trained to predict the blade root DELs and tower base DELs, respectively, using the RAWS, RATI, RAHS, and control setpoint variables as inputs. The Matlab Deep Learning Toolbox was used to create and train the ANNs (The MathWorks, 2021). The loss function is defined as the mean squared error, which is minimized using Bayesian regularization. The ANNs consist of a single hidden layer with 30 neurons, using hyperbolic tangent sigmoid activation functions.

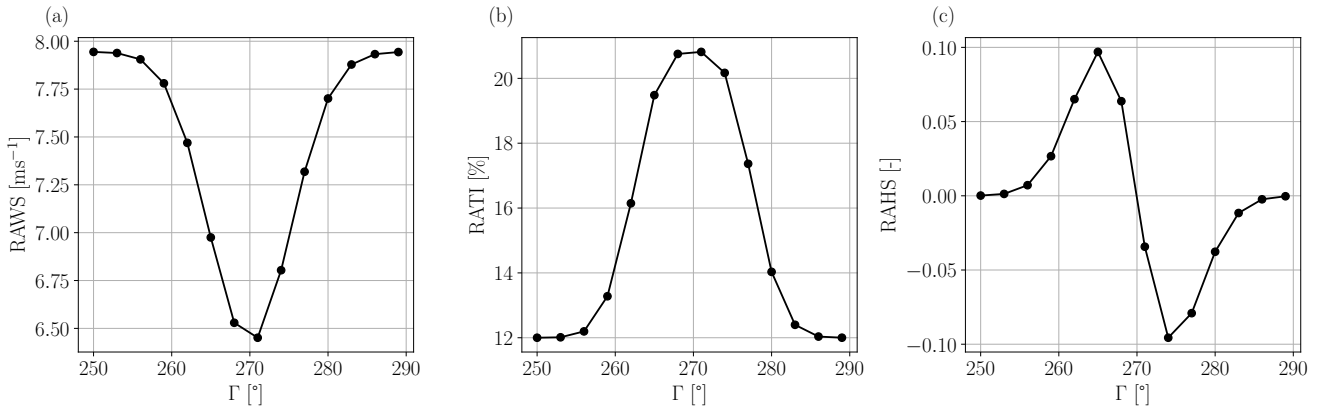


Figure 3. Example of the RAWs (left), RATI (middle), and RAHS (right) for a waked turbine for varying wind direction, for an ambient wind speed of 8 ms^{-1} and TI of 12% at a downstream distance of 6 diameters from the wake-shedding turbine. For a wind direction of 270° , the array of turbines is aligned with the incoming wind.

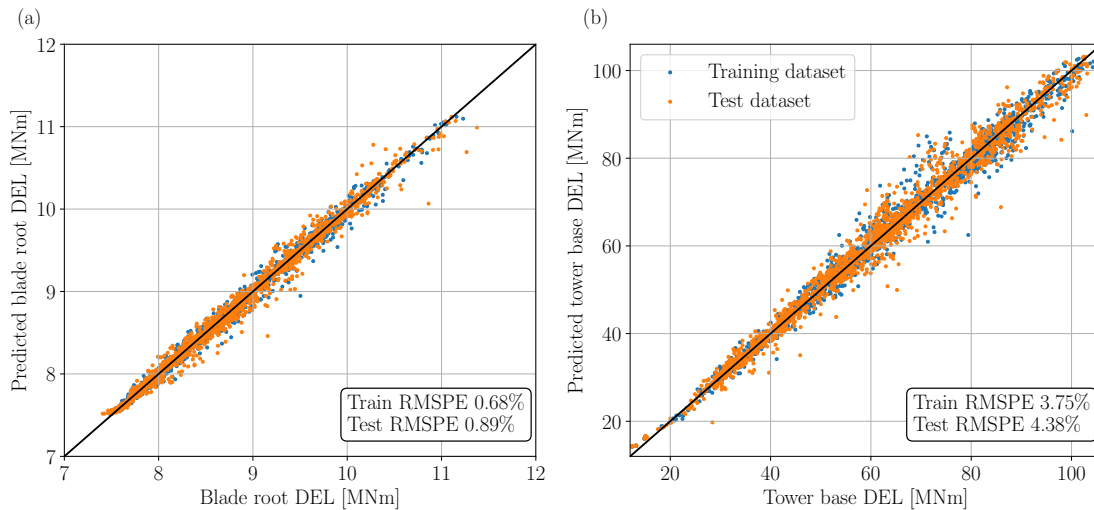


Figure 4. Performance of the load surrogate models for the projected blade root DELs (a) and projected tower base DELs (b) when the input RAIQs are estimated with FAST.Farm. Root-mean-square percentage errors (RMSPE) are used as performance metrics. Half of the dataset was used for the training of the ANN (in blue), while the other half was used for testing the trained ANN (in orange).

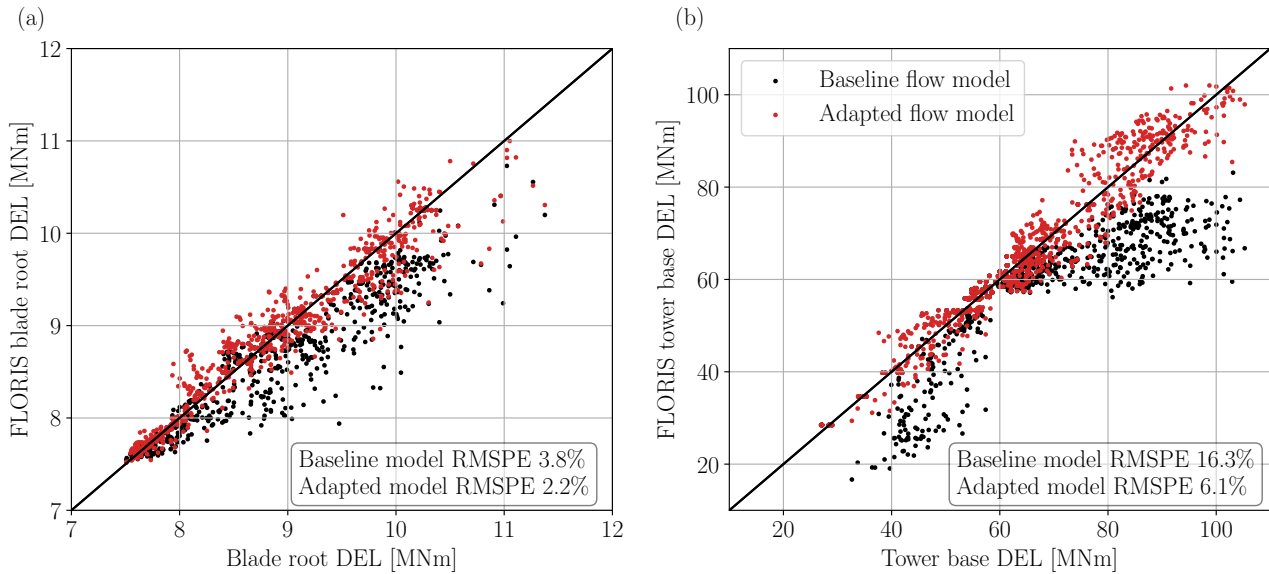


Figure 5. Predicted DELs when the RAIQs are computed from the FLORIS baseline (in black) and the calibrated wind farm flow models (in red). The plots include both the training and testing datasets, filtered for cases with $I = 12\%$. **(a)** Projected blade root DEL; **(b)** projected tower base DEL.

Figure 4 illustrates the performance of the load surrogate model when the inputs are directly estimated from FAST.Farm for both the training and testing datasets. The root-mean-square percentage error (RMSPE) is used as performance metric. The scatter plots for both the training and testing datasets are similar, indicating that the ANN training database was sufficiently large to ensure a correct generalization.

Figure 5 visualizes the performance of the combined engineering wake and load surrogate models. As discussed in Sect. 3.1, load estimates based on RAIQs from FLORIS in its baseline configuration were not satisfactory. To address this problem, the wake-added turbulence model in FLORIS was replaced with the Ishihara and Qian (2018) model, and the “wind farm as a sensor” was used for calibrating all model parameters. The training data for this calibration came from the previously described set of FAST.Farm simulations. A maximum likelihood approach was used to identify the correction of wake model parameters, based on a cost function combining the residuals for power and RATI. To illustrate the tuning improvements, Fig. 5 compares the estimated DELs using the load surrogate linked with the baseline version of FLORIS (shown as black dots) with the ones obtained with the calibrated flow model (shown as red dots). The results show considerable improvements. In particular, panel (b) highlights the impact of the flow model adjustments, as the baseline model significantly underpredicts the tower base loads. This is primarily due to the crude estimation of RATI in the baseline model, which uses the Crespo et al. (1996) model.



3.3 Damage model

The load model provides a set of DELs for each site ambient condition in \mathbf{W}_a . However, DELs are primarily representative quantities used to compare the effects of different operational conditions. To quantify the actual impact on each component, DELs must be converted into mechanical fatigue damage, which must then be aggregated across the range of ambient wind and operating conditions experienced over the lifetime of the turbine.

Accurately estimating the actual damage suffered by a component requires detailed information about its shape, geometry, and structural characteristics. However, such level of detail is beyond the scope of this work. Therefore, here we adopt the approach outlined in Hayman G. J. and Buhl M. Jr. (2012), where the fatigue damage $D_{\Delta t}^c$ for a given equivalent load $DEL_{\Delta t}^c$ over the time duration Δt can be calculated as

$$D_{\Delta t}^c = \frac{(DEL_{\Delta t}^c)^m \cdot N_{\Delta t}^{eq}}{(2 \cdot L_u)^m} \quad \forall c \in C, \quad (8)$$

where L_u represents the ultimate load obtained using the material stress curve (Pacheco et al., 2022).

3.4 Economic model

The economic model estimates the net economic profit by combining revenue from power production with cost from fatigue damage. The net economic profit is calculated as the difference between the accrued revenue and the incurred cost over the wind farm lifetime T .

The revenue model estimates the economic value of supplying the wind farm power to the electricity grid as

$$\text{Revenue}(\mathbf{W}_a, \mathbf{u}) = \mathbb{R}_1(\mathbf{W}_a) \cdot \sum_{i=1}^N P_i(\mathbf{W}_a, \mathbf{u}), \quad (9)$$

where \mathbb{R}_1 is the electricity market price, the total power yield of the wind farm is $\sum_{i=1}^N P_i$, and P_i denotes the power generated by i -th turbine. Electricity market prices are volatile and vary across years and regions. The power output of the wind farm directly influences these pricing patterns, especially as the share of wind power in total generation increases (Kölle et al., 2022; Seel et al., 2021; Loth et al., 2022; Swisher et al., 2022; Canet et al., 2023; Kainz et al., 2024). During periods of high wind generation, energy prices typically decrease. Any additional power generated by the wind farm during these hours results in lower revenue, creating a negative correlation between wind farm yield and market price.

While the relationship between wind conditions and spot-market prices is complex, as discussed in Kölle et al. (2022), a simplified model is used in this work. This model captures the dependency of market price on ambient wind speed through a polynomial equation, which is sufficient to represent the observed negative correlation (Canet et al., 2023; Kainz et al., 2024). The following expression is considered in this work,

$$\mathbb{R}_1(\mathbf{W}_a) = \mathbb{R}_{\text{avg}} \cdot (r_1 \cdot U^3 + r_2 \cdot U^2 + r_3 \cdot U + r_4), \quad (10)$$

where r_{1-4} denote the parameters of the third order polynomial. A best fit was obtained using the MATLAB Curve Fitting Toolbox (The MathWorks Inc., 2022). Historical spot-market prices from the German energy market, along with the ambient



wind speed data from a wind farm in the same market region, were used as input for the regression. For improved accuracy, the electricity market price was normalized by the annual average price \mathbb{R}_{avg} , as discussed in Kainz et al. (2024). For details
 330 regarding regression performance, refer to Kainz et al. (2024).

The second component of the profit equation is the cost model, which estimates the maintenance expenses arising from accumulated damage to the components of each turbine in the wind farm. Maintenance costs are generally divided into two categories: scheduled (preventive) maintenance, and unscheduled (corrective) maintenance (DIN Standard 13306:2018, 2018).

Scheduled maintenance involves routine tasks carried out according to a predetermined time plan, often through continuous
 335 or periodic monitoring of turbine components. Unscheduled maintenance, on the other hand, is performed after a failure occurs and the operational readiness of the component needs to be restored. Unscheduled maintenance can also be opportunistic, prompted by condition monitoring to prevent imminent failure.

Walgern et al. (2017) provides a summary of both maintenance categories. Maintenance costs are primarily driven by factors such as equipment repair or replacement costs, the number of technicians required for repairs, failure rates, and operational
 340 downtime losses. Scheduled maintenance costs are generally easier to estimate, as they are based on a predefined maintenance plan. In contrast, unscheduled maintenance costs depend on stochastic factors such as mean time between failures, component reliability, and repair time per failure (Frank De Jong, 2007).

This work considers a simplified maintenance cost model, which aims to capture only the fundamental aspects of the complex, variable, and uncertain annual O&M cost. The formulation is inspired by the discussions in TotalControl (2022a), Bakhshi
 345 and Sandborn (2018), Poore (2008), and Frank De Jong (2007). The incurred maintenance cost can be written as

$$\text{Cost}(\mathbf{W}_a, \mathbf{u}) = \sum_c \frac{\mathbb{C}_{\text{opex}}^c(\mathbf{W}_a)}{D_{\text{ref}}^c} \cdot \sum_{i=1}^N D_i^c(\mathbf{W}_a, \mathbf{u}), \quad (11a)$$

where

$$\mathbb{C}_{\text{opex}}^c(\mathbf{W}_a) = \mathbb{C}_1^c \cdot [(\mathbb{R}_1(\mathbf{W}_a) \cdot \text{CF} \cdot \sum_{i=1}^N \mathbb{C}_{3,i}^c \cdot P_i^r) + \mathbb{C}_5^c] + \mathbb{C}_2^c \cdot [(\mathbb{R}_1(\mathbf{W}_a) \cdot \text{CF} \cdot \sum_{i=1}^N \mathbb{C}_{4,i}^c \cdot P_i^r) + \mathbb{C}_6^c]. \quad (11b)$$

For a given component c , the operation and maintenance expense $\mathbb{C}_{\text{opex}}^c$ is composed of fixed and variable cost items.
 350 The fixed costs, denoted as \mathbb{C}_{5-6}^c , account for the average repair cost, including equipment, labor, and operational personnel expenses. The variable costs represent the opportunity cost incurred due to production losses during turbine maintenance.

In Eq. (11b), the first cost item, consisting of parameters \mathbb{C}_1^c , \mathbb{C}_3^c , and \mathbb{C}_5^c , corresponds to the scheduled maintenance expenses. The second cost item, consisting of parameters \mathbb{C}_2^c , \mathbb{C}_4^c , and \mathbb{C}_6^c , corresponds to the unscheduled maintenance expenses.

The opportunity cost in the variable component is estimated as the product of the electricity market price \mathbb{R}_1 , the average
 355 downtime for the component \mathbb{C}_{3-4}^c due to turbine maintenance, and the average wind farm yield. The average yield is calculated as the product of the sum of the rated power output P_i^r of all turbines multiplied by the wind farm capacity factor CF.

The O&M expense is then linearly amortized over the reference damage D_{ref}^c to determine the maintenance cost due to the incurred damage D_i^c . The total maintenance cost is obtained by summing the costs for each individual component.

The final estimated net economic profit represents the optimization objective, as shown in Eq. (1a). It should be noted that
 360 the economic merit function used in this study is a simplified version sourced from the open literature. While this provides for



a useful simple approximation, it is essential to acknowledge that wind farm operators and developers, with access to more detailed operational data, are in a much better position to create more precise cost models.

4 Results and discussion

To evaluate the benefits of the proposed formulation through an application scenario, WFC is deployed on an existing wind farm. The wind farm

- is considered to have already operated for half of its target operational life T of 20 years, and
- it has accrued additional unexpected damage over this duration, which would lead to premature component failure if the operation continued as usual.

In this approach, the lifetime-aware formulation is applied to the remaining lifespan of the assets, taking into account the current state of health resulting from accumulated damage. The proposed formulation focuses on component failure due to accumulated fatigue at the blade root and tower base. These locations were chosen based on the critical nature of the components and the significant maintenance costs the wind farm operator would face in the event of failure (Anand et al., 2022; Canet et al., 2021; Stehly et al., 2020). Additionally, in the experimental validation of the lifetime-aware WFC formulation, Braunbehrens et al. (2024) limited the fatigue damage assessment to these two components due to technical limits in the scaled turbine models. Results revealed that both the tower base and blade root exhibit distinct responses to varying inflow and control conditions.

Any component failure leads to maintenance and downtime, as outlined in Sect. 3.4. For simplicity, it is assumed that the fixed costs associated with maintenance, downtime, and the number of maintenance activities remain constant over time, although this is not really true according to the classical bathtub curve. To evaluate lifetime quantities, rather than simulating the entire operational life of the wind farm using time series of wind conditions, only a single year is considered. It is assumed that the ambient wind conditions for this year are representative of the conditions for the remaining years. The set of ambient wind conditions \mathbf{W}_a over the operational lifespan T – comprising individual wind condition bins, $\mathbf{W}_a^{\text{bin}}$, and their corresponding probabilities of occurrence, f_a^{bin} – is derived from the site wind rose.

In the case studies presented here, only yaw-misalignment-based wake-steering WFC is considered. Therefore, the decision variables in the proposed optimization problem (Eq. 1) are limited to the yaw-offset set points, $\mathbf{u} = \boldsymbol{\gamma} = [\gamma_1, \dots, \gamma_i, \dots, \gamma_N]$. The bounds on the yaw-offsets, as defined in Eq. (1c), are constrained to a limiting value of $\pm 20^\circ$.

The relevant model parameters, including those for the economic model, are detailed in Tab. 1. The maintenance cost parameters are derived from the values reported in Poore (2008); Sheng (2013); Pfaffel et al. (2017); Chan and Mo (2017); Cevasco et al. (2021), which are based on various databases also referenced in Bakhshi and Sandborn (2018).



Table 1. Overview of the cost items for the maintenance expense model. Cost parameters are derived from values reported in the following references: Sheng (2013); Cevasco et al. (2021); Pfaffel et al. (2017); Chan and Mo (2017); Poore (2008); Bakhshi and Sandborn (2018).

Cost item	Description	Category	Unit	Value tower	Value blade	Scheduled
C_1	Number of downtimes	Variable	-	5	5	✓
C_2				0.02	0.05	✗
C_3	Downtime duration	Variable	hours	96	192	✓
C_4						✗
C_5	Average cost of repair	Fixed	Euro/kW	3	3	✓
C_6				5	5	✗

4.1 Reference control formulations

390 In addition to the proposed formulation, referred to as “*Max-profit*”, five alternative WFC strategies are used for comparison. These include greedy control, power-boosting control, and three load-aware formulations that account for component damage. A brief description of each of the considered WFC strategies is provided below.

1. The first reference formulation represents the state-of-the-art operation for most existing wind farms. In this approach, each turbine within the farm operates independently from the others by orienting its nacelle to face the local wind direction. This formulation serves as a baseline for comparison and will henceforth be referred to as “*Greedy*”.

2. The second reference formulation corresponds to the classical wake-steering strategy to maximize AEP (Campagnolo et al., 2020; Göçmen et al., 2022). The unconstrained optimization problem

$$\max_{\mathbf{u}} \sum_T \sum_{i=1}^N P_i(\mathbf{W}_a, \mathbf{u}) \quad (12)$$

maximizes the overall farm power output and, in turn, the accrued revenue. This formulation will henceforth be called “*Max-power*”.

3. The third reference formulation builds on the second one by limiting the loading on the turbine components. The strategy is adapted from the formulations discussed in TotalControl (2022b) and Eguinoa et al. (2021).

The optimization problem can be expressed as

$$\max_{\mathbf{u}} \sum_T \text{Revenue}(\mathbf{W}_a, \mathbf{u}), \quad (13a)$$

subject to

$$D_i^c(\mathbf{W}_a^{\text{bin}}, \mathbf{u}) \leq \mathbb{K}_1 \cdot \max_i D_i^c(\mathbf{W}_a^{\text{bin}}) \quad \forall i \in N \quad \forall \text{bin} \in \mathbf{W}_a \quad \text{and} \quad \forall c \in C. \quad (13b)$$

The damage limit for a given component c is defined as the maximum damage observed across all turbines in the baseline formulation, scaled by a factor \mathbb{K}_1 . Parameter \mathbb{K}_1 represents the safety factor typically applied during the turbine design



410 phase to account for additional loading during operation and all other uncertainties. The damage limit is set individually for each ambient wind condition bin $\mathbf{W}_a^{\text{bin}}$ within the full set of wind conditions, \mathbf{W}_a . This formulation will henceforth be referred to as “*Load-constrained*”.

4. The fourth reference formulation balances the power production and the incurred loading of different components. The formulation has been adopted from the discussions in Harrison et al. (2020a), Bossanyi (2018), and Kanev et al. (2018). The resulting optimization problem can be expressed as

415
$$\max_{\mathbf{u}} \sum_T \left(\mathbb{W}_P \cdot \sum_{i=1}^N P_i(\mathbf{W}_a, \mathbf{u}) - \sum_{c=1}^C \mathbb{W}_D^c \cdot \max_i D_i^c(\mathbf{W}_a, \mathbf{u}) \right). \quad (14)$$

In this formulation, the optimization problem maximizes the total power generated by the wind farm, while minimizing the distribution of loading across individual turbines. The approach prioritizes turbines with a higher available fatigue budget, using them more than those with greater accumulated damage, thereby ensuring a more balanced load distribution throughout the farm. The function $\max_i D_i^c$ represents the maximum damage accrued across all turbines for a given component c . The weight parameters, \mathbb{W}_P and \mathbb{W}_D^c , are used to adjust the relative importance of the different components in the objective function. These parameters are fine-tuned through a parameter-sweep optimization, yielding the most optimal solution for the given set of ambient wind conditions, \mathbf{W}_a . This formulation will henceforth be referred to as “*Load-balance*”.

- 425 5. The fifth reference formulation is a modification of the proposed formulation, where though the optimization problem is subjected to a lifetime constraint, the optimization objective only aims to maximize revenue i.e. it simply writes

$$\max_{\mathbf{u}} \sum_T \text{Revenue}(\mathbf{W}_a, \mathbf{u}), \quad (15)$$

subject to Eq. (1b). This formulation will henceforth be referred to as “*Lifetime-revenue*”.

4.2 Case study I: Simple wind farm layout and synthetic wind rose

430 The first case study evaluates the performance characteristics of the proposed WFC formulation in comparison to reference control strategies, including the baseline, within a simplified setup. This study provides a comprehensive assessment of optimal yaw-offset schedules, power output, component loading, and their impact on lifetime economic performance in terms of revenue, cost, and profit across different WFC formulations. For this purpose, a simple wind farm configuration consisting of three turbines is considered, along with a simplified ambient wind condition subset derived from a synthetic wind rose.

435 The performance of the resulting optimal yaw-offset schedule is validated using FAST.Farm. As for the generation of the load surrogate model database, the turbulent ambient wind field is generated using the Kaimal model in TurbSim tool (Jonkman, 2016), with 24 turbulent seeds employed to ensure statistical convergence of the results. The yaw angles for each turbine are prescribed as fixed values from the look-up tables in the ElastoDyn module (Jonkman and Shaler, 2021).

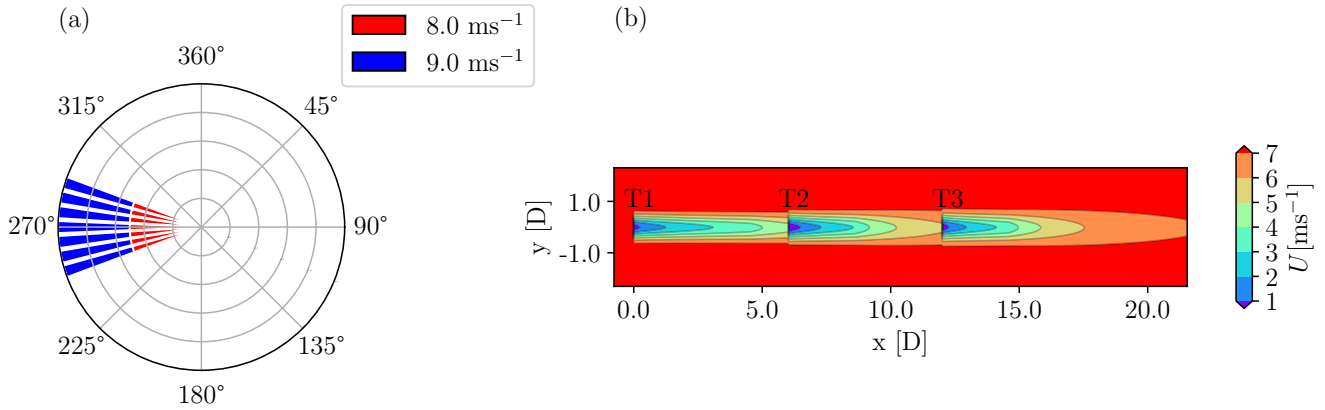


Figure 6. Layout and input wind conditions for the simplified case study setup. Wind rose showing ambient input wind speeds and directions (a). Wind farm layout and wakes at hub height for wind blowing from the western direction (b).

4.2.1 Layout and input wind conditions

The turbine layout resembles a typical WFC demonstrator case for wind tunnel experiments and simulations (Campagnolo et al., 2020). Aligned layouts are also studied in field tests (Göçmen et al., 2022). Here we consider three IEA 3.4 MW reference wind turbines, with a rated wind speed of 9.8 ms^{-1} (Bortolotti et al., 2019). Figure 6b shows the turbines T1, T2, and T3 in the aligned layout with 6-diameter-spacing between the turbines. This figure also shows the wakes in the fully aligned layout for a representative ambient wind condition for the baseline case, where all turbines point straight into the incoming wind.

The synthetic wind rose is shown in Fig. 6a, where the individual wind conditions, $\mathbf{W}_a^{\text{bin}}$, are assumed to have an equal probability of occurrence, f_a^{bin} . The purpose of selecting this wind rose is to evaluate the performance of different WFC strategies without the influence of the frequency distribution of the individual wind condition bins. The synthetic wind rose consists of wind direction sectors ranging from 250° to 290° , with the 270° direction aligning with the turbine layout. Each wind direction sector includes wind speeds of 8 and 9 ms^{-1} , each with equal probability. Under these conditions, the baseline *Greedy* formulation results in an overall wake loss of 11%.

For all WFC approaches, T1 and T2 perform wake steering according to their respective control policies, whereas T3 always operates in *Greedy* mode. Moreover, T2 is assumed to have accumulated in the first 10 years of operation 25% more damage to its components than anticipated.

4.2.2 Control schedule, power, and load distribution

Figure 7 displays the yaw-offset schedules derived from the different WFC formulations for an ambient wind speed of 8 ms^{-1} for turbines T1, T2, and T3, respectively from left to right. The x -axis represents the ambient wind direction sector Γ in degrees, while the y -axis indicates the optimal yaw-offset in degrees.

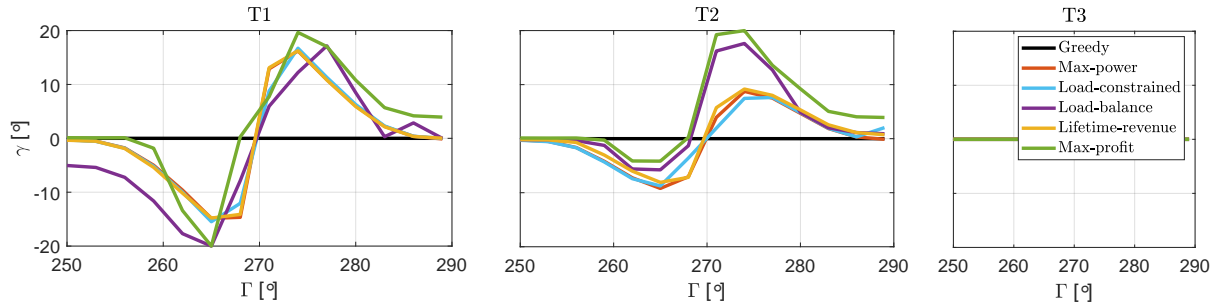


Figure 7. Yaw-offset schedules for T1, T2, and T3 as functions of all the wind direction sectors Γ , at an ambient wind speed of 8 ms^{-1} , for all the formulated WFC strategies. As wake steering is only implemented on T1 and T2, the yaw-offset of T3 is constant at 0° .

Figures 8, 9, and 10 present the resulting power, blade root DELs, and tower base DELs, respectively, obtained by applying the optimal yaw-offset schedules of each WFC formulation shown in Fig. 7. In each figure, the outputs are displayed as panels, with rows corresponding to the six WFC strategies and columns representing the three turbines. The y -axis shows the absolute value of the output in the respective units, and the x -axis shows the ambient wind direction sector Γ in degrees. Solid lines represent the measured outputs (labeled ‘Meas.’), while dashed lines show the corresponding predictions (labeled ‘Pred.’) obtained during the synthesis of the optimal yaw-offsets.

In all panels of Fig. 7, 8, 9, and 10, different colors are used to distinguish the outputs for the six WFC strategies: the baseline *Greedy* strategy in black, the *Max-power* strategy in orange, the *Load-constrained* strategy in blue, the *Load-balance* strategy in violet, the *Lifetime-revenue* strategy in yellow, and the proposed *Max-profit* strategy in green.

For all WFC strategies, turbines T2 and T3 operate within the wake of the upstream turbines, resulting in a reduced power output compared to T1, as shown in Fig. 8. In the baseline strategy, the power of the downstream turbines decreases as they enter partial wake conditions for $\Gamma \neq 270^\circ$, with the largest power loss occurring under full waking at $\Gamma = 270^\circ$. The power loss is most significant for T3, as it operates under the combined wakes of both upstream turbines. The power produced by the downstream turbines T2 and T3 is influenced by the available wind speed in the flow, which follows the trend of the RAWS, as shown in Fig. 3a.

Additionally, the blade root DELs for the baseline formulation show an asymmetric behavior with respect to the ambient wind direction, as seen in Fig. 9. For $\Gamma < 270^\circ$, the DELs of T2 and T3 are higher than those of T1, while for $\Gamma > 270^\circ$, the DELs of T2 and T3 are lower. This asymmetry is primarily driven by the corresponding RAHS, which also exhibits an asymmetric response with respect to Γ (see Fig. 3c).

In contrast, the tower base DELs for the baseline formulation display a symmetric behavior with respect to Γ , as shown in Fig. 10, with both T2 and T3 experiencing higher DELs than T1. This is because tower base DELs are mainly influenced by the RATI, which is higher for the waked turbines (see Fig. 3b) and exhibits a symmetric pattern with respect to Γ .

For an 8 ms^{-1} ambient wind speed, as shown in Fig. 7, all WFC formulations result in similar yaw-offsets for T1. The yaw-offsets for T1 are generally higher in magnitude than those for T2, as T1 operates in clean inflow conditions, which are

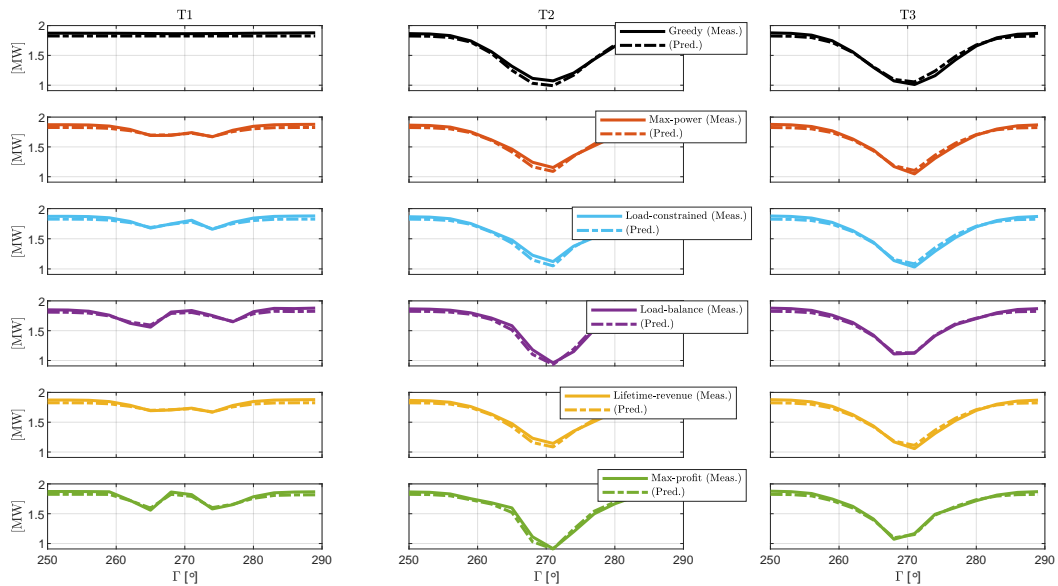


Figure 8. Power output for case study I. The three columns from left to right denote the outputs of the three turbines, T1, T2, and T3, respectively. The six rows from top to bottom denote the six control formulations. In every panel, the x -axis shows the input wind direction Γ , the y -axis shows the generated power, the solid curves show the measured value from FAST.Farm, and the dashed curves show the corresponding value predicted by the optimization framework.

typically associated with lower total loading compared to the waked inflow conditions experienced by T2. Consequently, T1 has a larger available budget to accommodate additional load increases due to active wake steering, resulting in larger yaw-offsets compared to T2.

485 For T1, the four damage-aware formulations – *Load-constrained*, *Load-balance*, *Lifetime-revenue*, and *Max-profit* – result in slightly lower yaw-offsets compared to the *Max-power* strategy. However, for T2, these damage-aware strategies lead to more aggressive wake steering for $\Gamma > 270^\circ$ and less aggressive steering for $\Gamma < 270^\circ$ compared to the *Max-power* strategy. This is because the yaw schedules are primarily influenced by the blade loads, which exhibit an asymmetric behavior with respect to Γ . As a result, it is beneficial to employ more aggressive wake steering for $\Gamma > 270^\circ$ as it reduces blade root DELs, while for
 490 $\Gamma < 270^\circ$ wake steering increases these same loads.

Compared to the baseline, all other WFC strategies result in a slight decrease in power for T1 and an increase in power for T2 and T3, as shown in Fig. 8. Consequently, all WFC strategies lead to an overall power gain for the wind farm. Additionally, a comparison between the solid and dashed lines for all strategies reveals that the measured turbine power outputs closely align with the estimated values. This high level of accuracy is due to the precise estimation of RAWs by the engineering flow model
 495 used within the optimization framework (refer to Sect. 3.1 for details). Since RAWs is the primary driver of power production,

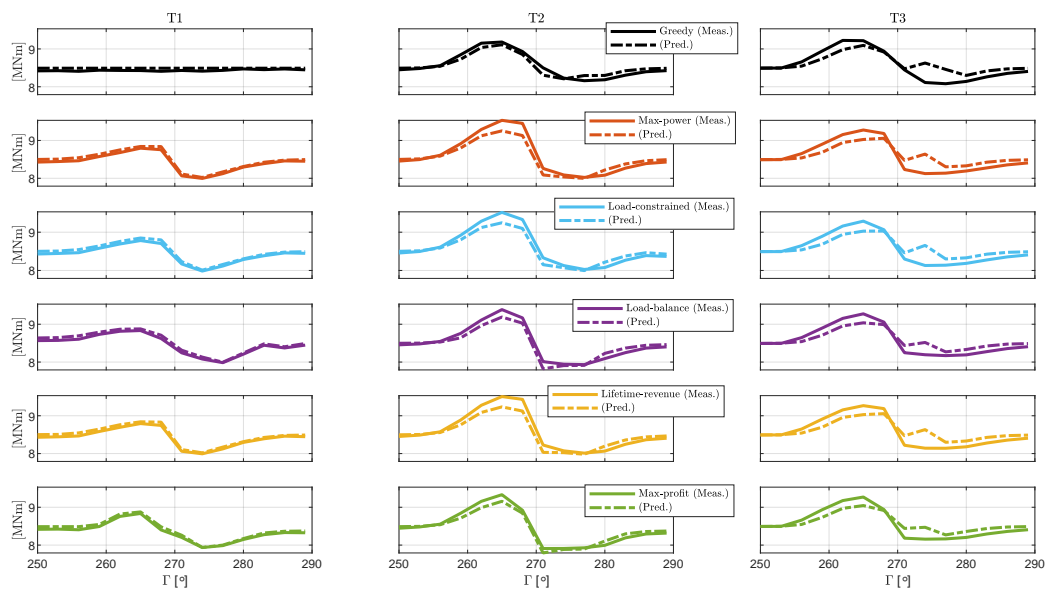


Figure 9. Blade root projected DELs for case study I.

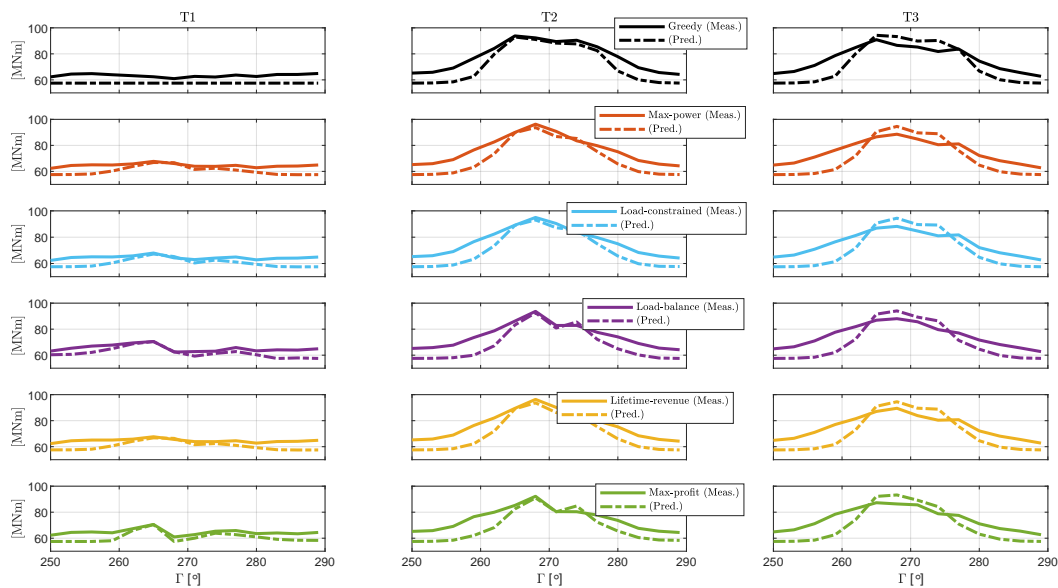


Figure 10. Tower base projected DELs for case study I.



the predicted power closely matches the measured one for the yawed turbine T1, the waked turbine T3, and the yawed and waked turbine T2.

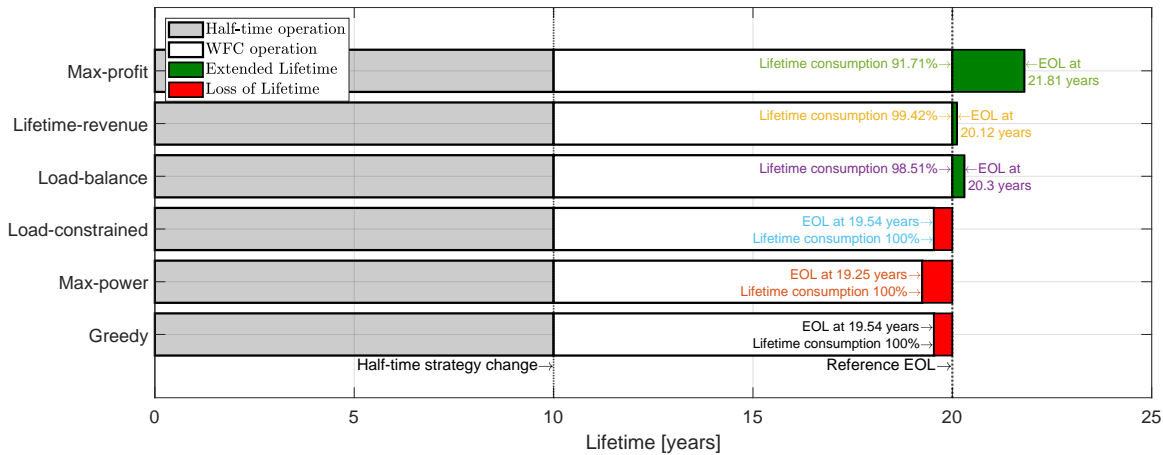
Active wake control leads to an increase in blade root DELs for all turbines when $\Gamma < 270^\circ$, and a slight decrease in DELs for $\Gamma > 270^\circ$, as shown in Fig. 9. The variation in blade root DELs is most significant for T2, as it experiences the combined effects of operating in a waked inflow and performing wake steering. Additionally, a comparison of the solid and dashed lines indicates that the blade root DELs are well predicted by the optimization framework (cf. Sect. 3.2.3), which effectively captures the trends in load variation with respect to Γ , for T1 (yawed), T3 (waked), and T2 (yawed and waked). This accuracy is especially important for load-aware strategies, where the optimal yaw offset is directly influenced by these variations in load.

For tower base loading, as shown in Fig. 10, active wake control leads to a slight increase in DELs for the yawed turbine, while significantly reducing DELs for the downstream turbines. Since tower base DELs are primarily driven by the RATI, deflections of the upstream wake results in lower RATIs for the downstream turbines, leading to reduced loading. Additionally, a comparison of the solid and dashed lines reveals that, for all control strategies, tower loads are consistently under-predicted in partial wake conditions ($\Gamma < 265^\circ$ and $\Gamma > 275^\circ$) and over-predicted in full wake conditions ($265^\circ \leq \Gamma \leq 275^\circ$). However, the optimization framework still captures the trends in tower load variation accurately. This observed mismatch is primarily attributed to the presence of rotor up-tilt in FAST.Farm, which leads to vertical wake displacement and vertical shear at the rotor inflow. Since FLORIS does not account for vertical shear, the predictions from the optimization framework slightly differ from those obtained from FAST.Farm. Despite this, the under- and over-predictions generally cancel each other out for the inflow conditions considered in this case study. The impact of this small net prediction mismatch on lifetime performance is discussed in the following section.

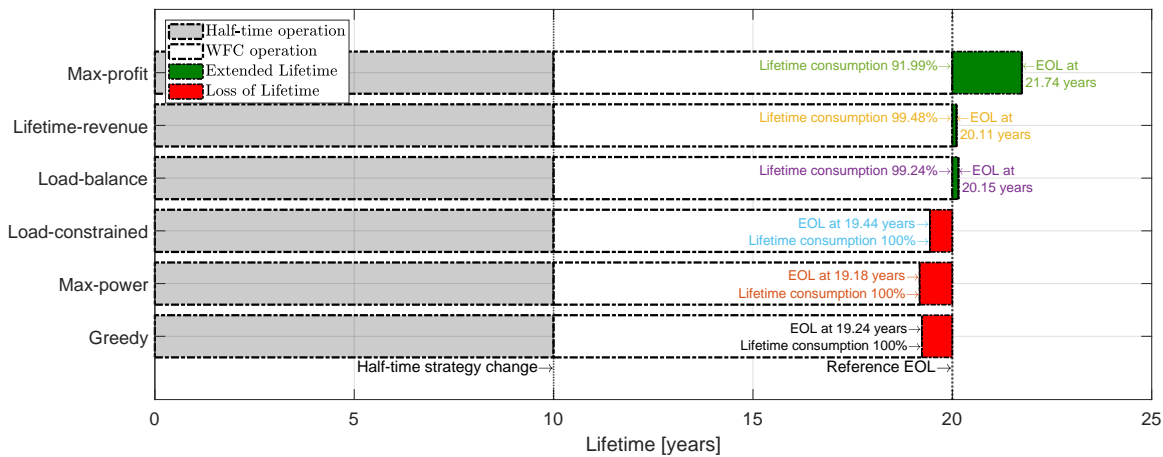
4.2.3 Lifetime consumption

Figure 11 illustrates the lifetime consumption of the wind farm across all considered WFC strategies. Lifetime consumption is determined by the accumulated fatigue damage on the components, with the wind farm reaching its EOL when any component on any turbine reaches its EOL. A component reaches its EOL when the accumulated damage D (cf. Sect. 3.3) equals 1, which corresponds to a lifetime consumption of 100%. Figure 11a displays the lifetime consumption resulting from the application of optimal yaw-offsets in the validation case study, while Fig. 11b shows the expected lifetime consumption predicted by the optimization framework. In both figures, lifetime consumption is represented as horizontal bars, with each bar corresponding to a specific WFC strategy. The x -axis represents time in years, and the y -axis lists the six WFC strategies. As detailed in Sect. 4.2.2, the performance of the wind farm is assessed over a 20-year operational life (reference EOL). The WFC strategies are implemented after the wind farm has operated under the baseline strategy for 10 years (half-time strategy change). Consequently, each bar is divided into shaded regions representing four distinct phases:

- The grey region indicates the lifetime consumed while operating without any optimal yaw-offset (baseline strategy).
- The white region represents the lifetime consumed while operating with the different WFC strategies.
- The red region denotes the lost lifetime of the wind farm when the EOL is reached before the reference EOL.



(a) Measured



(b) Predicted

Figure 11. Lifetime consumption of the wind farm for all the WFC strategies for case study I. The solid outline of the horizontal bars in panel (a) denotes the measured value based on FAST.Farm, and the dashed outline in panel (b) denotes the corresponding predicted value from the optimization framework.

- The green region represents the gained or extended lifetime, where the consumed life until the reference EOL was less than 100%. The remaining useful life is linearly extrapolated to estimate the additional operational years.

A close examination of Fig. 11a reveals that, when operating under the *Greedy*, *Max-power*, and *Load-constrained* strategies, the wind farm fails to reach the reference EOL, resulting in a loss of operational years. In contrast, the remaining strategies – *Load-balance*, *Lifetime-revenue*, and *Max-profit* – operate in a more damage-aware manner, leading to a gain in operational years beyond the reference EOL. The *Max-power* strategy yields the shortest operational life. This suggests that, while the



535 aggressive wake steering employed in the *Max-power* strategy (as seen in the orange line plots in Fig. 7) may enhance energy
production, it also accelerates fatigue accumulation, even surpassing the accumulation seen in the baseline (no wake steering)
case. This outcome is primarily due to the combination of increased fatigue from the pre-damage scenario and the aggressive
wake steering implemented on T2 to boost the yield of T3. As a result of its own activity, T2 experiences a significant increase
in blade root DELs, which is not offset by the modest decrease due to the wake steering of T1, as discussed in Sect. 4.2.2.
540 Consequently, the wind farm suffers higher fatigue damage, leading to a reduction in operational life.

The *Load-constrained* strategy results in a less aggressive yaw-offset schedule compared to the *Max-power* strategy. This
is because the optimization constraints defined in Eq. (13b), which account for the loading in individual wind condition bins
 W_a^{bin} , are rarely active. However, as discussed in Sect.1, the fatigue budget for a specific W_a^{bin} does not only depend on the
fatigue damage accumulated within that bin, but also on the damage accumulation from other wind condition bins that the wind
545 farm is exposed to. In other words, from a wind farm lifetime perspective, the control actions for a given wind input condition
in load-aware operation are influenced by the relative impact of this condition in relation to others. Since the *Load-constrained*
formulation only considers individual bins, it overlooks the cumulative effects of other wind condition bins, which ultimately
results in a loss of lifetime.

While the *Load-balance* strategy ensures that the wind farm reaches its reference EOL, the optimal balance between fatigue
550 accumulation and energy yield extends the remaining useful life of the wind farm, allowing it to operate beyond its original
operational lifetime. However, because the optimization formulation (see Eq. 14) does not explicitly impose constraints to
guarantee a desired lifetime, the observed performance can be attributed to the optimal tuning of weights to maximize the
overall objective. For more complex farm layouts and inflow conditions, this formulation may not ensure the wind farm will
operate over a specific lifetime, despite the use of optimized weight tuning.

555 As anticipated, the *Lifetime-revenue* strategy ensures that the wind farm reaches the desired operational life. This is because
the strategy accounts for the combined loading from all wind conditions the farm experiences throughout its lifetime, while
simultaneously optimizing farm power and, consequently, revenue, for each individual wind condition bin.

The proposed *Max-profit* formulation, in addition to explicitly considering lifetime constraints, finds the most profitable way
of operating the assets throughout their lifetime. It does so by not only focusing on the power output of the individual turbines,
560 but also considering the total energy yield and balancing it against the operational and maintenance (O&M) costs resulting
from accumulated damage. Compared to the *Lifetime-revenue* formulation, the *Max-profit* strategy adopts a more aggressive
wake steering in partial wake overlap conditions ($260^\circ < \Gamma < 280^\circ$) for T1, implements one-sided wake steering for $\Gamma > 270^\circ$
to reduce blade root DELs, while avoiding wake steering altogether for $\Gamma < 270^\circ$. This results in an optimal balance between
accumulated damage and revenue, enabling the wind farm to operate for the desired duration while maximizing economic
565 profit throughout its operational life.

Figure 11b shows the estimated lifetime consumption based on the predicted blade root DELs (dashed curves in Fig. 9)
and tower base DELs (dashed curves in Fig. 10) for all the WFC strategies. The predicted lifetime consumption is visually
represented in the same way as the calculated lifetime consumption in Fig. 11a. However, the predicted lifetime consump-
tion features dashed outlines around the horizontal bars, highlighting the expected performance, while the measured lifetime



570 consumption is shown with solid outlines. By comparing the two figures, it is clear that the optimization framework predicts lifetime consumption with reasonable accuracy. The remaining useful life is only slightly underpredicted compared to the validation case study. The minor prediction mismatches across different wind direction sectors Γ , as shown in Fig. 9 and Fig. 10, have minimal impact on the overall lifetime consumption and remaining useful life.

4.2.4 Lifetime economic performance

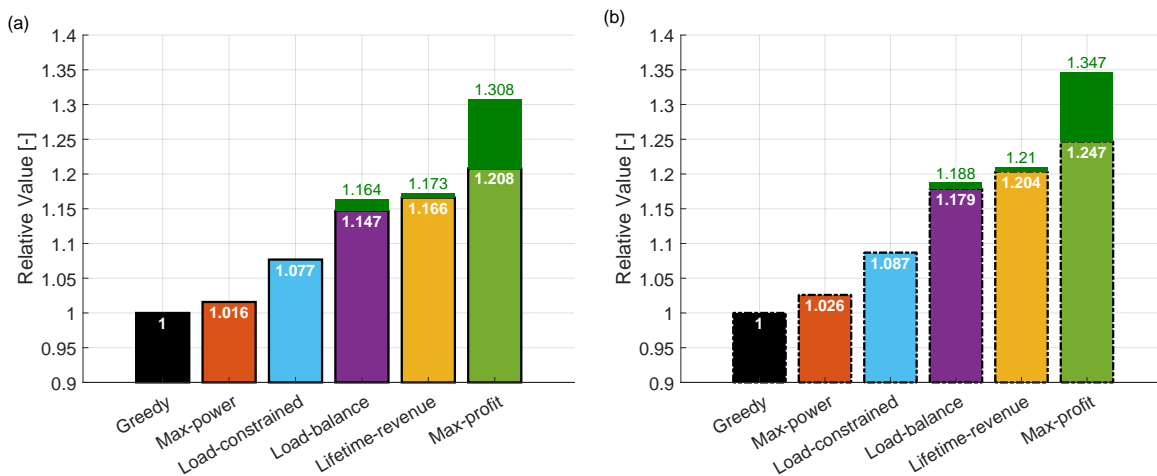


Figure 12. Lifetime profit of the wind farm for all the WFC strategies for case study I. The economic profit is calculated as the difference between accrued revenue and the sum of incurred cost and lost revenue. The solid outline of the vertical bars in panel (a) denotes the measured value based on FAST.Farm, and the dashed outline in panel (b) denotes the corresponding predicted value from the optimization framework.

575 Figure 12 illustrates the economic performance of the wind farm over its lifetime. Fig. 12a shows the economic profit obtained by applying the optimal yaw-offsets in the validation case study, while Fig. 12b displays the expected economic profit as predicted by the optimization framework. In both figures, the vertical bar plots represent the economic profit. This is calculated as the difference between the economic revenue from wind farm yield and the sum of economic costs from O&M and the loss of lifetime. The x -axis shows the different WFC strategies and the y -axis represents the relative economic profit compared to the baseline. The numbers written in white on the bars indicate the relative values over the 20-year operational duration. Additionally, some strategies include stacked green bars, which represent the extra economic gain due to lifetime extension. The corresponding numbers written in green denote the additional profit assuming the wind farm continues to operate beyond its reference EOL.

580 Figure 12a shows that all WFC strategies result in higher economic profit compared to the baseline formulation. The magnitudes of these profits are notably higher for the damage-aware strategies. This demonstrates that incorporating damage considerations into the WFC optimization problem – whether accurately or through approximations – has a significant impact on lifetime economic profit.



Both the *Max-power* and *Load-constrained* strategies experience a loss of lifetime, leading to a reduction in revenue. The *Max-power* strategy suffers a larger loss due to its shorter operational life. The *Load-constrained* strategy, on the other hand, incurred smaller economic costs due to slightly lower damage accumulation. As a result, the *Max-power* strategy only achieves a 1.7% increase in profit, while the *Load-constrained* strategy sees a 7.7% increase.

The *Load-balance* strategy, due to its optimal tuning of weights in the optimization objective, results in an additional 7% profit over the *Load-constrained* strategy. The *Lifetime-revenue* strategy further optimizes loading over all various operating conditions simultaneously, maximizing revenue and leading to a profit increase of 16.5% over the baseline.

Finally, the proposed *Max-profit* formulation ensures the wind farm meets the desired lifetime while maximizing profit. Although it generates less revenue than the *Lifetime-revenue* strategy, it saves significantly on maintenance expenses due to a reduced accumulated damage. This results in an additional 4% profit compared to the *Lifetime-revenue* strategy.

The importance of optimizing profit, rather than solely focusing on revenue maximization, is further emphasized by the additional profit gained from the extension of the operational life of the wind farm. The *Max-profit* formulation achieves a 30% profit gain over the baseline, and an additional 13% gain compared to the *Lifetime-revenue* strategy.

Similarly to the prediction of lifetime consumption, the expected lifetime profit shown in Fig. 12b is quite accurately predicted by the optimization framework. The dashed outline in the vertical bars in Fig. 12b represents the expected value, while the solid outline in the bars in Fig. 12a corresponds to the measured values. When comparing the two figures, it is evident that there is a slight overprediction of lifetime profit for all WFC strategies compared to the respective baseline. This overprediction can be attributed to the increased reduction in costs achieved by the optimization framework, which results from the overprediction of component loads.

4.2.5 Uncertainty quantification

Due to the uncertainties associated with lifetime fatigue damage estimation, their impact on O&M costs, and the regulations governing wind farm market participation, the economic lifetime-aware WFC optimization problem (refer to Sect. 2 for details) is inherently stochastic. While the underlying models in the optimization framework use deterministic inputs and outputs, the resulting lifetime profit from power generation and damage accumulation can vary significantly. This variation may lead to different optimal yaw-offset schedules.

Figure 13a illustrates the uncertainty in lifetime profit resulting from economic model uncertainty (cf. Sect. 3.4). This uncertainty is represented as a vertical bar plot. The y -axis shows the relative lifetime profit compared to the baseline case, while the x -axis denotes different WFC strategies. For each vertical bar, the numbers from top to bottom represent the upper bound, average, and lower bound of the lifetime profit uncertainty, respectively.

The uncertainty is calculated by varying all the economic model parameters, assuming a uniform distribution. These parameters include thirteen economic model factors across two components. Four parameters are related to the mean time to maintenance (both scheduled and unscheduled), four are related to downtime for repair and maintenance, four pertain to personnel/labor costs for maintenance, and one is associated with the electricity market price. Uncertainty quantification is per-

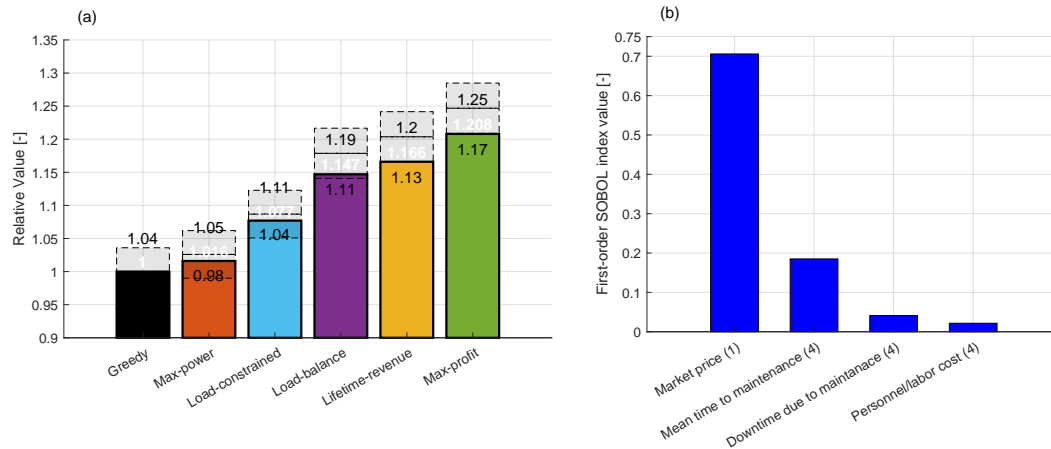


Figure 13. Quantification of the uncertainties on lifetime economic performance caused by uncertainties in the economic model parameters of Sect. 3.4. Results of standard Monte Carlo analysis for a uniformly distributed economic parameter space for the proposed *Max-profit* strategy, where the numbers on the bars in white denote the mean value and the numbers in black on the dashed boxes denote the corresponding uncertainty bounds (a). Results of variance-based parametric sensitivity analysis for the proposed *Max-profit* strategy, where the vertical bars represent the SOBOL index for different categories (b).

formed using Monte Carlo analysis. In this approach, numerous evaluations are conducted by randomly sampling the parameter space and evaluating the merit function until convergence is achieved.

The results in Fig. 13a show that, for all WFC strategies, a maximum variation of 8% in the parameters leads to uncertainties varying only between 3% to 4%. This indicates that the lifetime profit is only modestly affected by the uncertainties in the economic parameters across all control strategies.

Additionally, a variance-based parameter sensitivity analysis is conducted for the *Max-profit* strategy, where the thirteen economic model parameters are varied to better understand the sources of uncertainty in the lifetime profit. The results of the sensitivity analysis are presented in terms of first-order sensitivity coefficients, also known as first-order SOBOL indices (Saltelli et al., 2010). The sensitivity coefficient S_{X_k} indicates how much the output variance $\text{Var}(Y)$ can be reduced, on average, if the uncertainty associated with the input variable X_k is fully known, where $Y = f(X_1, X_2, \dots, X_k, \dots)$.

Figure 13b displays the sensitivity analysis results. The economic model parameters are grouped into four qualitative categories, which are shown along the x -axis. The number in parentheses next to each category indicates the number of parameters in that group. The vertical bars represent the SOBOL index for each category, and the y -axis shows the corresponding values.

From the figure, it is clear that the uncertainty in electricity market prices contributes most significantly to the overall uncertainty. This is because market prices directly affect both the accrued revenue and the lost revenue due to downtime. The second largest source of uncertainty is the mean time to maintenance, which represents the time to failure. While the remaining

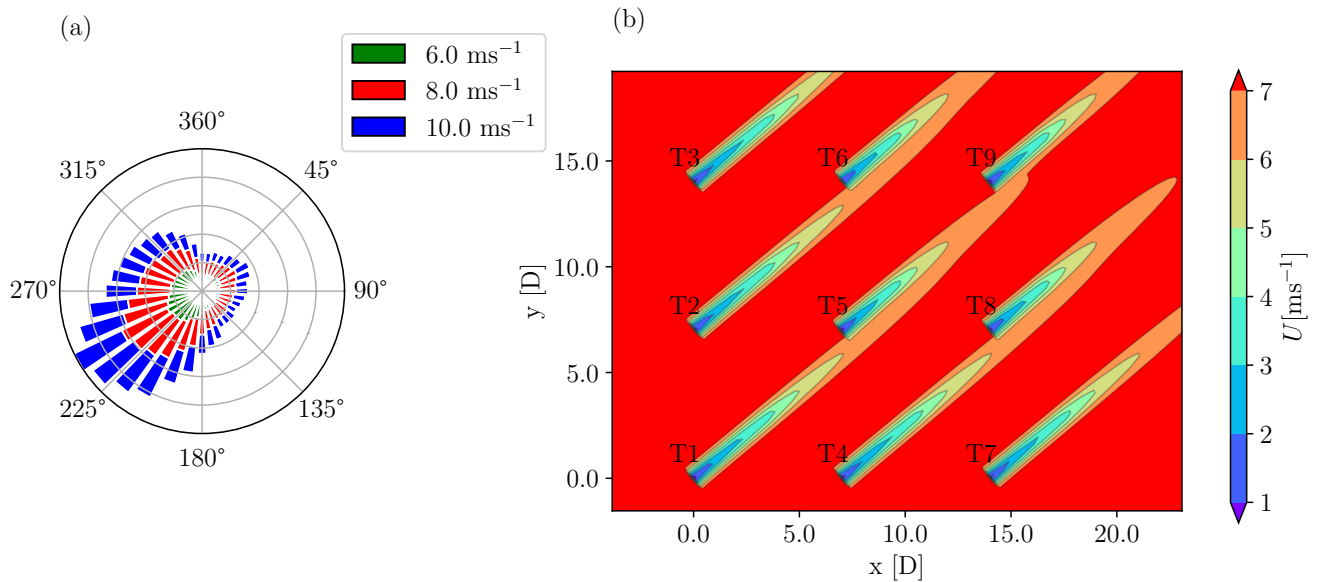


Figure 14. Layout and wind conditions for the realistic case study. Wind rose (a). Wind farm layout and wakes at hub height for wind blowing from the southwestern direction (b).

two categories contribute relatively less, their absolute impact is still noteworthy. This further emphasizes the importance of quantifying the uncertainties associated with failure rates and other O&M parameters.

4.3 Case study II: Realistic wind farm layout and wind rose

640 The goal of the second case study is to apply the proposed WFC approach to a more complex scenario. In this case, the wind farm is a small offshore cluster operating under realistic wind conditions. The primary objective is to evaluate how the new method performs for a larger cluster of turbines, focusing on how the increased turbine count and varied inflow conditions affect the solution. Additionally, this case study aims to assess the growth of the computational cost of the proposed method as the wind farm cluster size increases.

645 For comparison, all reference control formulations presented in Sect. 4.1 are also considered here. The results shown in the following are those obtained by the optimization framework. Since the previous results showed that the optimization framework provides accurate predictions of lifetime quantities, additional validation using FAST.Farm was deemed not necessary.

4.3.1 Layout and input wind conditions

This case considers the nine-turbine wind farm layout defined in the CL-Windcon project (Irigoyen, 2017). The turbines are arranged in a regular grid, with a spacing of 7 D in the x -direction and 5 D in the y -direction, as shown in Fig. 14b. The wind conditions are based on reanalysis data obtained from the site of the Hollandse Kust Nord offshore wind farm (Hersbach et al., 2020), which is also being assessed as part of the SUDOCO project (Gebraad et al., 2024). The corresponding wind rose is

shown in Fig. 14a. The wind speed range is limited between 6 and 10 ms^{-1} . It is assumed that these wind conditions remain constant over the course of the year.

655 Since the wind inflow comes from all directions, all turbines operate in a combination of waked and free-stream conditions. The baseline AEP loss due to wake interaction, as calculated by FLORIS, is approximately 5%. Similarly to case study I, the market price is assumed to vary around an annual average, depending on the ambient wind speed. An annual inflation rate of 8% is applied for the economic evaluation. For simplicity, the number of maintenance activities, fixed maintenance costs, and maintenance downtime per component are assumed to remain constant over time. Additionally, the lifetime consumption is
 660 calculated based on damage accumulation at the tower base and blade root.

This case study assumes a 20-year lifetime. During the first 10 years, the farm operates in greedy control mode, before switching to one of the tested control formulations for the second half of the lifetime. As in case study I, one turbine (T5) is assumed to have accumulated more fatigue damage than the others. T5 operates in waked conditions most of the time, and also wakes the turbines at the trailing edge of the farm. As a result, it is assumed that after 10 years turbine T5 will have accumulated
 665 75% more damage than expected. This additional damage is greater than in case study I, as the more realistic wind conditions in this study are less challenging than focusing on a single wind sector. This is clearly an idealized exemplary situation. In another scenario, T5 might represent a machine that suffers from higher failure rates than the others, for example because of malfunctioning issues, extra vibrations suffered during erections, or other possible reasons.

4.3.2 Lifetime consumption

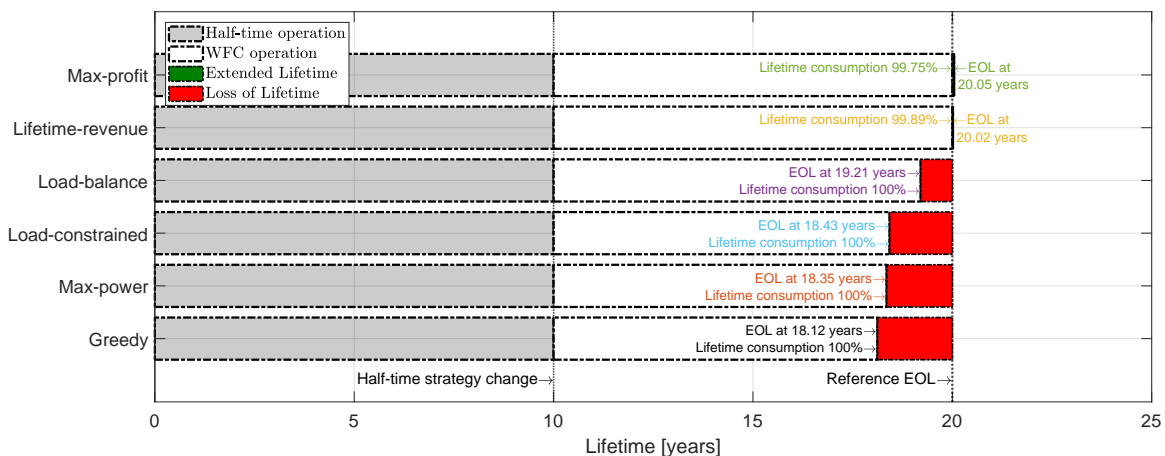


Figure 15. Lifetime consumption of the wind farm for all the WFC strategies for case study II.

670 Figure 15 shows the lifetime consumption for the wind farm across all WFC strategies. Similarly to Fig. 11b, the horizontal bars represent the operational years of the wind farm, with a reference EOL of 20 years. As previously noted, the WFC strategies are deployed after the first 10 years of operation.



The green-shaded region indicates the extended lifetime years beyond the reference EOL, while the red-shaded region represents the loss of operational years due to lifetime consumption before the reference EOL. For a more detailed interpretation of the layout of the figure, please refer to Sect. 4.2.3.

Figure 16 shows that, compared to the baseline, all other WFC strategies result in a larger number of operational years. Strategies that account for component damage over the lifetime – either explicitly or indirectly – also lead to increased operational years compared to the baseline and *Max-power* strategies. However, only the lifetime-aware strategies, specifically *Lifetime-revenue* and *Max-profit*, ensure operation throughout the entire reference EOL. This is because the optimal yaw offset for these two strategies is less aggressive, as they consider the inflow and operational conditions at all turbines over their entire lifetime. Furthermore, the proposed *Max-profit* formulation provides a slight lifetime extension, allowing the wind farm to operate beyond the reference EOL, thus generating additional revenue.

4.3.3 Lifetime economic performance

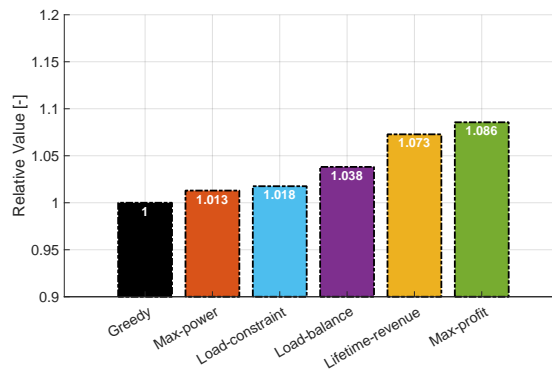


Figure 16. Lifetime profit of the wind farm for all the WFC strategies for case study II. The economic profit is calculated as the difference between accrued revenue and the sum of incurred cost and lost revenue.

Figure 16 presents the lifetime economic performance of the wind farm. The results are displayed in the same format as in Fig. 12b. The vertical bars show the lifetime profit relative to the baseline profit for all the formulated WFC strategies. The numbers written in white on the bars represent the relative profit values over the 20-year operational duration.

All strategies result in economic gains over the baseline for the considered scenario. However, due to lifetime loss, the *Max-power*, *Load-constrained*, and *Load-balance* strategies show relatively minor gains, which depend on the corresponding revenue loss. In contrast, the two lifetime-aware strategies – *Lifetime-revenue* and *Max-profit* – yield significantly higher gains of 7.3% and 8.6%, respectively, thanks to their guaranteed operation over the full lifetime.

The difference in gains between these two strategies highlights the importance of balancing economic costs and revenue within the optimization objective of the proposed *Max-profit* formulation. Additionally, the profit gain magnitude is influenced by wake interactions across the farm over its entire lifetime.



4.4 Computational effort

695 The proposed methodology requires a setpoint optimization for all turbines in all possible ambient wind conditions throughout their entire lifetime. The resulting one-shot optimization can become computationally demanding. To assess the growth of the computational cost, the layout shown in Fig. 14b is expanded to include more turbines.

Starting with the 3×3 layout, the configuration is reduced to a 2×2 setup and then extended to 4×4 and 5×5 configurations, all while maintaining the same x - y separation distances. The other problem parameters (wind rose, EOL, time of deployment
700 of WFC, etc.) are unvaried with respect to the 3×3 case.

The optimization problem is solved iteratively until numerical convergence is achieved. All optimizations are performed on a desktop computer with an Intel(R) Core(TM) i7 processor, 8 GB of RAM, and a 64-bit operating system.

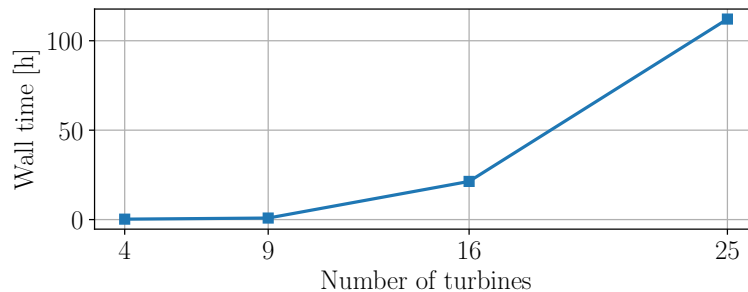


Figure 17. Increase of wall time with the number of turbines in a regular grid with spacings of 7 D and 5 D in the x - and y -directions, respectively.

Figure 17 presents the results of the computational performance test. The x -axis represents the total number of turbines in the assessed configuration, while the y -axis shows the real clock time taken by the optimization problem to converge. As
705 expected, the proposed methodology is computationally expensive, with the computational cost increasing significantly as the wind farm size grows. For instance, the optimization on a 5×5 layout takes approximately 100 hours. However, since the optimization is performed offline, the problem only needs to be solved once throughout the lifetime of the wind farm, either before or during the operational phase. As a result, the computational effort, relative to the operational lifetime of the wind farm, is negligible. Even if the wind farm operator decides to update the optimal yaw-offsets based on more accurate data, such
710 as actual damage measurements or digital twins, the computational cost of reevaluating the optimization problem will still be minimal compared to the operational duration. It is also important to note that no special efforts were made to optimize the code for computational efficiency, and only a standard desktop computer was used for the optimization which is not realistic for a large industrial project.

More importantly, the large increase in economic profit made possible by the proposed *Max-profit* strategy – compared to
715 the state-of-the-art *Max-power* and other simple strategies (as discussed in Sect. 4.2.4 and Sect. 4.3.3) – justifies the additional computational effort.



5 Conclusions

We have introduced a novel approach: economic lifetime-aware WFC. The new method integrates the current damage state of turbines – either obtained through a digital twin or estimated from operational data – to derive control policies that optimize the long-term lifetime management of the wind farm. The optimization is driven by an economic value function that balances power generation (considering fluctuating spot market prices) with O&M costs, including potential revenue losses due to turbine downtime. The optimization is constrained to ensure that the target lifetime of selected turbine components is met while operating under varying inflow conditions. The optimization variables include the control setpoints of each turbine, which can include axial induction, wake steering, mixing, or combinations thereof. In this sense, the proposed method is general, allowing end-users to select based on the availability or technical applicability of the different control approaches. The resulting optimal setpoints depend on the ambient wind conditions and are interpolated at run time based on the detected current conditions.

To implement our new proposed method, first, an engineering flow model is adapted to estimate the power output of each individual turbines within a wind farm for given wind climate conditions. Next, a load surrogate model uses the estimated rotor inflow to predict the DELs for selected turbine components, which are then accumulated into a representative damage value. Finally, an economic model integrates energy production with the cost of component fatigue damage to estimate the net profit, providing a comprehensive view of the economic performance of the wind farm.

The proposed lifetime-aware strategy, termed *Max-profit*, has been compared to five relevant reference formulations. The first two, *Greedy* and *Max-power*, do not account for loads. The following two, *Load-constrained* and *Load-balance*, incorporate loads by considering DELs either as a constraint or as an objective. The fifth formulation, *Lifetime-revenue*, is an intermediate formulation that considers the lifetime damage constraint but does not account for load-induced costs. The performance of the proposed formulation and the reference ones was evaluated through two different case studies using wake steering. The designed life of the wind farm is considered to be 20 years, and the control strategies are deployed after 10 years of baseline operation.

The first case study examined a simple wind farm layout consisting of three wind turbines and a synthetic wind rose. For validation, the mid-fidelity wind farm simulation tool FAST.Farm was used with multiple turbulent seed realizations. Results indicated that non-load-aware strategies lead to increased damage accumulation, causing the wind farm to prematurely reach its EOL, in turn resulting in reduced revenue. In contrast, all load-aware strategies are able to decrease lifetime consumption, leading to lower costs, smaller revenue losses, and higher profits. However, only the lifetime-aware strategies, *Lifetime-revenue* and *Max-profit*, ensure full operation throughout the desired lifetime duration. Additionally, in some case we observed an even longer lifetime, allowing for operation beyond the defined EOL, thereby generating additional profit.

Results also show accurate predictions of lifetime performance using the developed optimization framework. Furthermore, uncertainties in lifetime profit due to variations in the economic model parameters were assessed using Monte Carlo analysis, and variance-based parametric sensitivity analysis with first-order SOBOL indices. Results indicate that even with an 8% variation in all economic model parameters, lifetime profit uncertainties remain within 3%, while market price uncertainty has a more significant impact.



The second case study expanded the analysis to a larger wind farm cluster of nine turbines, typical of an onshore wind farm, arranged in a regular grid layout. This study also incorporated a real wind rose based on measured data. The results highlight the clear advantages of explicitly incorporating lifetime constraints into the WFC optimization problem. Specifically, only the *Lifetime-revenue* and *Max-profit* formulations were able to ensure operation over the entire desired lifetime. As damage accumulates over time, the control actions taken today – through the loading on the turbines – directly impact the available capacity for future control decisions. Since the other strategies do not explicitly account for the interplay between present and future control actions, they lead to higher fatigue accumulation and, ultimately, to a reduction in operational life. In contrast, the proposed *Max-profit* strategy results in approximately 8.6% higher profit compared to the baseline, with 1.3% of that increase attributed solely to the consideration of maintenance expenses in the optimization process.

760 Additionally, we also assessed the computational burden of solving the proposed optimization problem, which performs a one-shot optimization over the defined lifetime for all inflow conditions. This was carried out on a standard desktop computer, rather than using high-performance computing resources, without any attempt at optimizing for computational efficiency. For a wind farm with 25 turbines arranged in a regular grid layout, the optimization process took over 100 hours to converge. The computational load increases significantly as the size and complexity of the wind farm grows. However, since the optimization is performed offline once and then rarely (if ever) repeated, the computational burden is minimal in the context of the typical operational lifespan of a wind farm, which spans several years.

770 The proposed formulation can be utilized as a decision support tool during the pre-deployment phase to evaluate the economic feasibility of various wind farm operational scenarios. For instance, an operator could compare the trade-offs between a shorter plant lifetime driven by higher power capture (which also results in greater loading and increased O&M costs) followed by early decommissioning, versus extending the lifetime of the plant beyond its original design by adopting a more conservative power capture strategy and reducing turbine loading. Once an optimal life management strategy has been selected, the wind farm operator can deploy the lifetime-aware controller to maximize profit while ensuring that the specified lifespan targets for turbine components are met.

Appendix A: Nomenclature

775	c	Turbine component
	C	Number of turbine components
	C	Cost item
	D	Damage
	D_{ref}	Damage threshold
780	f_a	Wind condition frequency
	I	Turbulence intensity
	k_*	Flow model parameter
	\mathbb{K}_1	Damage safety factor



	L	Load cycle amplitude
785	L_u	Ultimate load
	m	Wöhler exponent
	n	Number of load cycles
	N	Number of turbines
	N_{eq}	Equivalent number of load cycles
790	P	Turbine power
	P^r	Turbine rated power
	r	Rotor radial coordinate
	r	Polynomial fit parameter
	R	Rotor radius
795	\mathbb{R}_1	Electricity market price
	T	Turbine lifetime
	U	Wind speed
	u	Control set-point
	\mathbf{W}_a	Set of ambient wind conditions
800	\mathbb{W}	Weight parameter for <i>Load balance</i> strategy
	α	Induction factor
	γ	Yaw angle
	Γ	Wind direction
805	Δt	Time duration
	ψ	Rotor azimuthal coordinate
	AEP	Annual energy production
	ANN	Artificial neural network
810	CF	Capacity factor
	DEL	Damage equivalent load
	EOL	End of life
	FLORIS	FLOW Redirection and Induction in Steady State
	O&M	Operation and maintenance
815	RAWS	Rotor-average wind speed
	RATI	Rotor-average turbulence intensity
	RAHS	Rotor-average horizontal shear
	RAIQ	Rotor-average inflow quantity



	RMSPE	Root mean square percentage error
820	TI	Turbulence intensity
	WFC	Wind farm control

Data availability. The content and data of figures 3-5, 7-13, and 15-17 can be retrieved in Python pickle format via the DOI¹: <https://doi.org/10.5281/zenodo.15118524>

825 *Author contributions.* CLB developed the concept of economic lifetime-aware WFC and supervised the overall research. AA and RB expanded the concept, performed literature research, and developed the methodology. AA and RB implemented the proposed method using the models discussed in the optimization framework section. AG developed the load surrogate and supported AA and RB with its integration into the framework. AA, RB, and AG carried out the validation studies, where AG performed the FAST.Farm simulations. All authors contributed to the interpretation of the results. AA, RB and CLB prepared the manuscript, with contributions from AG in load surrogate and results
830 and discussion sections. All authors provided valuable input to this research work through discussions, feedback, and improvement of the manuscript.

Competing interests. The authors declare that they have no conflict of interest, except for CLB who is the Editor-in-Chief of the Wind Energy Science journal.

Financial support. This work has been supported by the SUDOCO and TWAIN projects, which receive funding from the European Union's
835 Horizon Europe Programme under the grant agreements No. 101122256 and 101122194, respectively.

Acknowledgements. The authors would like to thank S. Kainz for the valuable support with the uncertainty quantification study.

¹Review note: This is a preliminary repository, the final DOI will be generated if the paper is accepted



References

- Anand, A., Loew, S., and Bottasso, C. L.: Economic nonlinear model predictive control of fatigue for a hybrid wind-battery generation system, *Journal of Physics: Conference Series*, 2265, 032 106, <https://doi.org/10.1088/1742-6596/2265/3/032106>, 2022.
- 840 Bakhshi, R. and Sandborn, P.: Overview of Wind Turbine Field Failure Databases: A Discussion of the Requirements for an Analysis, <https://doi.org/10.1115/POWER2018-7311>, 2018.
- Bastankhah, M. et al.: A new analytical model for wind-turbine wakes, *Renewable energy*, 2014.
- Bortolotti, P., Tarres, H., Dykes, K., Merz, K., Sethuraman, L., Verelst, D., and Zahle, F.: IEA Wind TCP Task 37: Systems Engineering in Wind Energy - WP2.1 Reference Wind Turbines, <https://doi.org/10.2172/1529216>, 2019.
- 845 Bossanyi, E.: Combining induction control and wake steering for wind farm energy and fatigue loads optimisation, *Journal of Physics: Conference Series*, 1037, 032 011, <https://doi.org/10.1088/1742-6596/1037/3/032011>, 2018.
- Bossanyi, E.: Surrogate model for fast simulation of turbine loads in wind farms, *Journal of Physics: Conference Series*, 2265, 042 038, <https://doi.org/10.1088/1742-6596/2265/4/042038>, 2022.
- 850 Bottasso, C., Cacciola, S., and Schreiber, J.: Local wind speed estimation, with application to wake impingement detection, *Renewable Energy*, 116, 155–168, 2018.
- Braunbehrens, R., Vad, A., and Bottasso, C. L.: The wind farm as a sensor: learning and explaining orographic and plant-induced flow heterogeneities from operational data, *Wind Energy Science*, 8, 691–723, 2023.
- Braunbehrens, R., Anand, A., Campagnolo, F., and Bottasso, C. L.: First experimental results on lifetime-aware wind farm control, *Journal of Physics: Conference Series*, 2767, 032 042, <https://doi.org/10.1088/1742-6596/2767/3/032042>, 2024.
- 855 Campagnolo, F., Weber, R., Schreiber, J., and Bottasso, C. L.: Wind tunnel testing of wake steering with dynamic wind direction changes, *Wind Energy Science Discussions*, 2020, 1–33, 2020.
- Canet, H., Loew, S., and Bottasso, C. L.: What are the benefits of lidar-assisted control in the design of a wind turbine?, *Wind Energy Science*, 6, 1325–1340, <https://doi.org/10.5194/wes-6-1325-2021>, 2021.
- Canet, H., Guilloré, A., and Bottasso, C. L.: The eco-conscious wind turbine: design beyond purely economic metrics, *Wind Energy Science*, 8, 1029–1047, <https://doi.org/10.5194/wes-8-1029-2023>, 2023.
- 860 Cevasco, D., Koukoura, S., and Kolios, A. J.: Reliability, availability, maintainability data review for the identification of trends in offshore wind energy applications, *Renewable and Sustainable Energy Reviews*, 136, 110 414, <https://doi.org/10.1016/j.rser.2020.110414>, 2021.
- Chan, D. and Mo, J.: Life Cycle Reliability and Maintenance Analyses of Wind Turbines, *Energy Procedia*, 110, 328–333, <https://doi.org/10.1016/j.egypro.2017.03.148>, 2017.
- 865 Crespo, A., Herna, J., et al.: Turbulence characteristics in wind-turbine wakes, *Journal of wind engineering and industrial aerodynamics*, 1996.
- Damiani, R., Dana, S., Annoni, J., Fleming, P., Roadman, J., van Dam, J., and Dykes, K.: Assessment of wind turbine component loads under yaw-offset conditions, *Wind Energy Science*, 3, 173–189, <https://doi.org/10.5194/wes-3-173-2018>, 2018.
- Dimitrov, N. and Natarajan, A.: Wind farm set point optimization with surrogate models for load and power output targets, *Journal of Physics: Conference Series*, 2018, 012 013, <https://doi.org/10.1088/1742-6596/2018/1/012013>, 2021.
- 870 Dimitrov, N., Kelly, M. C., Vignaroli, A., and Berg, J.: From wind to loads: wind turbine site-specific load estimation with surrogate models trained on high-fidelity load databases, *Wind Energy Science*, 3, 767–790, <https://doi.org/10.5194/wes-3-767-2018>, 2018.



- DIN Standard 13306:2018: Maintenance - Maintenance terminology; Trilingual version EN: EN 13306:2012-02, <https://doi.org/10.31030/2641990>, 2018.
- 875 Eguinoa, I., Göçmen, T., Garcia-Rosa, P. B., Das, K., Petrović, V., Kölle, K., Manjock, A., Koivisto, M. J., and Smailes, M.: Wind farm flow control oriented to electricity markets and grid integration: Initial perspective analysis, *Advanced Control for Applications*, 3, <https://doi.org/10.1002/adc2.80>, 2021.
- Frank De Jong: Development of a model to estimate O&M costs for onshore wind farms, <https://api.semanticscholar.org/CorpusID:62623300>, 2007.
- 880 Gebraad, P., Kainz, S., Anand, A., Guilloré, A., Quick, J., and Gökhan, D.: Reference scenarios, SUDOCO deliverable repository, Horizon Europe Programme, Grant Agreement 101122256, SUDOCO, Brussels, Belgium, 2024.
- Göçmen, T., Campagnolo, F., Duc, T., Eguinoa, I., Andersen, S. J., Petrović, V., Imširović, L., Braunbehrens, R., Liew, J., Baungaard, M., et al.: FarmConnors wind farm flow control benchmark–Part I: Blind test results, *Wind Energy Science*, 7, 1791–1825, 2022.
- Guilloré, A., Campagnolo, F., and Bottasso, C. L.: A control-oriented load surrogate model based on sector-averaged inflow quantities: capturing damage for unawaked, waked, wake-steering and curtailed wind turbines, *Journal of Physics: Conference Series*, 2767, 032019, <https://doi.org/10.1088/1742-6596/2767/3/032019>, 2024.
- 885 Harrison, M., Bossanyi, E., Ruisi, R., and Skeen, N.: An initial study into the potential of wind farm control to reduce fatigue loads and extend asset life, *Journal of Physics: Conference Series*, 1618, 022007, <https://doi.org/10.1088/1742-6596/1618/2/022007>, 2020a.
- Harrison, M., Bossanyi, E., Ruisi, R., and Skeen, N.: An initial study into the potential of wind farm control to reduce fatigue loads and extend asset life, in: *Journal of Physics: Conference Series*, vol. 1618, p. 022007, IOP Publishing, 2020b.
- 890 Hayman G. J. and Buhl M. Jr.: MLife User’s Guide: A Tool for Computing Fatigue Loads and Statistics for Wind Turbines, Tech. Rep. NREL/TP-5000-59195, National Renewable Energy Laboratory (NREL), <https://www.nrel.gov/docs/fy13osti/59195.pdf>, 2012.
- Hersbach, H., Bell, B., Berrisford, P., Hirahara, S., Horányi, A., Muñoz-Sabater, J., Nicolas, J., Peubey, C., Radu, R., Schepers, D., et al.: The ERA5 global reanalysis, *Quarterly Journal of the Royal Meteorological Society*, 146, 1999–2049, 2020.
- 895 Howland, M. F., Lele, S. K., and Dabiri, J. O.: Wind farm power optimization through wake steering, *Proceedings of the National Academy of Sciences of the United States of America*, 116, 14 495–14 500, <https://doi.org/10.1073/pnas.1903680116>, 2019.
- IEC 61400-1, I. E. C.: IEC 61400-1: Wind Turbines - Part 1: Design Requirements, <https://webstore.iec.ch/publication/7103>, accessed: 2024-12-05, 2019.
- Irigoyen, U.: Definition of reference wind farms and simulation scenarios, CL-Windcon deliverable repository, European Horizon 2020 project, Report no. Ares(2017)5332644, CL-Windcon, Brussels, Belgium, 2017.
- 900 Ishihara, T. and Qian, G.-W.: A new Gaussian-based analytical wake model for wind turbines considering ambient turbulence intensities and thrust coefficient effects, *Journal of Wind Engineering and Industrial Aerodynamics*, 177, 275–292, 2018.
- Jonkman, B. J.: TurbSim User’s Guide: Version 2.00.00, Technical Report NREL/TP-5000-66123, National Renewable Energy Laboratory (NREL), <https://www.nrel.gov/docs/fy16osti/66123.pdf>, 2016.
- 905 Jonkman, J. and Shaler, K.: Fast.farm User’s Guide and Theory Manual, Technical Report NREL/TP-5000-78485, National Renewable Energy Laboratory (NREL), <https://www.nrel.gov/docs/fy21osti/78485.pdf>, 2021.
- Kainz, S., Guilloré, A., and Bottasso, C. L.: How do technological choices affect the economic and environmental performance of offshore wind farms?, *Journal of Physics: Conference Series*, 2767, 082005, <https://doi.org/10.1088/1742-6596/2767/8/082005>, 2024.
- Kanev, S. K., Savenije, F. J., and Engels, W. P.: Active wake control: An approach to optimize the lifetime operation of wind farms, *Wind Energy*, 21, 488–501, <https://doi.org/10.1002/we.2173>, 2018.
- 910



- Katic, I., Højstrup, J., and Jensen, N. O.: A simple model for cluster efficiency, in: European wind energy association conference and exhibition, pp. 407–410, A. Raguzzi, 1987.
- Kölle, K., Göçmen, T., Eguinoa, I., Alcayaga Román, L. A., Aparicio-Sanchez, M., Feng, J., Meyers, J., Pettas, V., and Sood, I.: FarmConnors market showcase results: wind farm flow control considering electricity prices, *Wind Energy Science*, 7, 2181–2200, <https://doi.org/10.5194/wes-7-2181-2022>, 2022.
- 915 Kretschmer, M., Jonkman, J., Pettas, V., and Cheng, P. W.: FAST.Farm load validation for single wake situations at alpha ventus, *Wind Energy Science*, 6, 1247–1262, <https://doi.org/10.5194/wes-6-1247-2021>, 2021.
- Larsen, G., Aagaard, M., and Bingøel, F.: Dynamic wake meandering modeling, Technical report, Technical University of Denmark (DTU), https://backend.orbit.dtu.dk/ws/portalfiles/portal/7703042/ris_r_1607.pdf, 2007.
- 920 Lee, J. C. and Fields, M. J.: An overview of wind energy production prediction bias, losses, and uncertainties, *Wind Energy Science Discussions*, 2020, 1–82, 2020.
- Liew, J., Riva, R., Friis-Møller, M., and Göçmen, T.: Wind farm control optimisation under load constraints via surrogate modelling, *Journal of Physics: Conference Series*, 2767, 092 039, <https://doi.org/10.1088/1742-6596/2767/9/092039>, 2024.
- Loth, E., Qin, C., Simpson, J. G., and Dykes, K.: Why we must move beyond LCOE for renewable energy design, *Advances in Applied Energy*, 8, 100 112, <https://doi.org/10.1016/j.adapen.2022.100112>, 2022.
- 925 Mendez Reyes, H., Kanev, S., Doekemeijer, B., and van Wingerden, J.-W.: Validation of a lookup-table approach to modeling turbine fatigue loads in wind farms under active wake control, *Wind Energy Science*, 4, 549–561, <https://doi.org/10.5194/wes-4-549-2019>, 2019.
- Meyers, J., Bottasso, C., Dykes, K., Fleming, P., Gebraad, P., Giebel, G., Göçmen, T., and van Wingerden, J.-W.: Wind farm flow control: prospects and challenges, *Wind Energy Science*, 7, 2271–2306, <https://doi.org/10.5194/wes-7-2271-2022>, 2022.
- 930 NREL: FLORIS: Version 3.2, GitHub repository, <https://github.com/NREL/floris>, 2022.
- Pacheco, J., Pimenta, F., Pereira, S., Cunha, Á., and Magalhães, F.: Fatigue Assessment of Wind Turbine Towers: Review of Processing Strategies with Illustrative Case Study, *Energies*, 15, 4782, <https://doi.org/10.3390/en15134782>, 2022.
- Pfaffel, S., Faulstich, S., and Rohrig, K.: Performance and Reliability of Wind Turbines: A Review, *Energies*, 10, 1904, <https://doi.org/10.3390/en10111904>, 2017.
- 935 Poore, R.: Development of an Operations and Maintenance Cost Model to Identify Cost of Energy Savings for Low Wind Speed Turbines: July 2, 2004 – June 30, 2008, <https://doi.org/10.2172/922541>, 2008.
- Porté-Agel, F., Bastankhah, M., and Shamsoddin, S.: Wind-Turbine and Wind-Farm Flows: A Review, 174, 2020.
- Saltelli, A., Annoni, P., Azzini, I., Campolongo, F., Ratto, M., and Tarantola, S.: Variance based sensitivity analysis of model output. Design and estimator for the total sensitivity index, *Computer Physics Communications*, 181, 259–270, <https://doi.org/10.1016/j.cpc.2009.09.018>, 2010.
- 940 Scheu, M. N., Kolios, A., Fischer, T., and Brennan, F.: Influence of statistical uncertainty of component reliability estimations on offshore wind farm availability, *Reliability Engineering & System Safety*, 168, 28–39, <https://doi.org/10.1016/j.res.2017.05.021>, 2017.
- Schreiber, J., Bottasso, C. L., and Bertelè, M.: Field testing of a local wind inflow estimator and wake detector, *Wind Energy Science*, 5, 867–884, <https://doi.org/10.5194/wes-5-867-2020>, 2020.
- 945 Seel, J., Millstein, D., Mills, A., Bolinger, M., and Wiser, R.: Plentiful electricity turns wholesale prices negative, *Advances in Applied Energy*, 4, 100 073, <https://doi.org/10.1016/j.adapen.2021.100073>, 2021.
- Shaler, K., Jasa, J., and Barter, G. E.: Efficient Loads Surrogates for Waked Turbines in an Array, *Journal of Physics: Conference Series*, 2265, 032 095, <https://doi.org/10.1088/1742-6596/2265/3/032095>, 2022.



- Sheng, S., ed.: Report on Wind Turbine Subsystem Reliability - A Survey of Various Databases (Presentation), <https://www.osti.gov/biblio/1090149>, 2013.
- 950 Stehly, T., Beiter, P., and Duffy, P.: 2019 Cost of Wind Energy Review, <https://doi.org/10.2172/1756710>, 2020.
- Stipa, S., Ajay, A., Allaerts, D., and Brinkerhoff, J.: The multi-scale coupled model: a new framework capturing wind farm–atmosphere interaction and global blockage effects, *Wind Energy Science*, 9, 1123–1152, <https://doi.org/10.5194/wes-9-1123-2024>, 2024.
- Sutherland, H. J.: On the Fatigue Analysis of Wind Turbines, <https://doi.org/10.2172/9460>, 1999.
- 955 Swisher, P., Murcia Leon, J. P., Gea-Bermúdez, J., Koivisto, M., Madsen, H. A., and Münster, M.: Competitiveness of a low specific power, low cut-out wind speed wind turbine in North and Central Europe towards 2050, *Applied Energy*, 306, 118043, <https://doi.org/10.1016/j.apenergy.2021.118043>, 2022.
- The MathWorks, I.: Deep Learning Toolbox: User’s Guide (r2018a), <https://de.mathworks.com/products/deep-learning.html>, accessed: 2024-12-05, 2021.
- 960 The MathWorks Inc.: Curve-fitting Toolbox (R2022b), <https://www.mathworks.com>, 2022.
- TotalControl: D2.1 Cost Model for fatigue degradation and O&M - Advanced integrated supervisory and wind turbine control for optimal operation of large Wind Power Plants: [TotalControl], <https://doi.org/10.3030/727680>, 2022a.
- TotalControl: D2.3 Optimization of WPP set-points, <https://doi.org/10.3030/727680>, 2022b.
- van den Broek, M. J., Becker, M., Sanderse, B., and van Wingerden, J.-W.: Dynamic wind farm flow control using free-vortex wake models, *Wind Energy Science*, 9, 721–740, <https://doi.org/10.5194/wes-9-721-2024>, 2024.
- 965 Walgern, J., Peters, L., and Madlener, R.: Economic Evaluation of Maintenance Strategies for Offshore Wind Turbines Based on Condition Monitoring Systems, *SSRN Electronic Journal*, <https://doi.org/10.2139/ssrn.3240555>, 2017.
- Wilkinson, M. R., Hendriks, B., Spinato, F., Gomez, E., Bulacio, H., Roca, J., Tavner, P., Feng, Y., and Long, H.: Methodology and Results of the Reliawind Reliability Field Study, <https://durham-repository.worktribe.com/output/1159302>, 2010.